nature structural & molecular biology

ARTICLES

https://doi.org/10.1038/s41594-020-0397-5

Engineering and functionalization of large circular tandem repeat protein nanoparticles

Colin E. Correnti[1], Jazmine P. Hallinan[2], Lindsey A. Doyle[2], Raymond O. Ruff[1], Carla A. Jaeger-Ruckstuhl[1], Yuexin Xu[1], Betty W. Shen[2], Amanda Qu[2], Caley Polkinghorn[3], Della J. Friend[2], Ashok D. Bandaranayake[1], Stanley R. Riddell[1], Brett K. Kaiser[3]✉, Barry L. Stoddard[2]✉ and Philip Bradley[1,4]✉

Protein engineering has enabled the design of molecular scaffolds that display a wide variety of sizes, shapes, symmetries and subunit compositions. Symmetric protein-based nanoparticles that display multiple protein domains can exhibit enhanced functional properties due to increased avidity and improved solution behavior and stability. Here we describe the creation and characterization of a computationally designed circular tandem repeat protein (cTRP) composed of 24 identical repeated motifs, which can display a variety of functional protein domains (cargo) at defined positions around its periphery. We demonstrate that cTRP nanoparticles can self-assemble from smaller individual subunits, can be produced from prokaryotic and human expression platforms, can employ a variety of cargo attachment strategies and can be used for applications (such as T-cell culture and expansion) requiring high-avidity molecular interactions on the cell surface.

TRPs are proteins that contain multiple repeated peptide sequences, usually spanning between 20 and 40 residues each[1–3]. Such repeated sequences, which are found in approximately 15–25% of proteins in various organisms, form highly similar folded topologies that self-associate to form closed circular or open linear protein scaffolds. Naturally occurring TRPs have evolved to bind a wide range of protein and nucleic acid partners[3].

TRPs are attractive platforms for protein engineering because they are straightforward to redesign and often display several favorable biophysical properties, including high thermal stability and solubility and ease of expression[3]. Many engineering efforts using TRPs have aimed to improve their stability and folding properties, and to develop them as alternatives to antibodies as protein-binding reagents. For example, high-affinity binders of various protein targets have been created from ankyrin proteins (DARPins)[4], and designed RNA-binding proteins have been created from Pumilio/fem-3 (PUF) proteins[5]. The use of TRPs as scaffolds to host additional protein domains has also been demonstrated by inserting an enzyme into loops connecting adjacent repeats in an ankyrin consensus repeat protein[6]. In addition, new protein structures (both linear and cyclic) have been created by engineering TRPs containing leucine-rich repeats[7], tetratricopeptide repeats[8,9] and computationally designed repeats[10].

We previously described the development and experimental validation of a computational strategy for the de novo design of closed, cTRPs spanning symmetries that range from 3 up to 12 identical repeats[11]. In those constructs, each repeat was composed of 31–35 residues corresponding to a left-handed α-helical bundle. The designed proteins expressed at very high levels, were extremely thermostable and soluble and formed structures that corresponded closely to their original designs. On the basis of those results, we refined the physical terms used for design and created a considerably larger cTRP of sufficient size and repeat number to allow fusion of multiple copies of functional protein domains around their periphery at evenly spaced intervals and with precisely defined symmetry.

Results

De novo design. The initial designed protein, which we refer to as 'cTRP24', corresponds to a circular tandem repeat architecture containing 24 identical structural units, folded into a ring with a 100-Å (10 nm) outer diameter, a 60-Å inner diameter and a 20-Å thickness perpendicular to the plane of the ring (Fig. 1a). Each repeat is composed of an identical 33-residue sequence (Fig. 1b) folded into a left-handed bundle containing two antiparallel α-helices (Fig. 1c). The inner and outer helices are 13 and 14 residues in length, respectively, and are connected by a three-residue loop (spanning residues 17–19 in each repeat). Twenty-four identical copies of that loop are all located on the same side of the model. An additional series of identical three-residue loops (spanning residues 1–3 in each repeat) are located on the opposing surface of the cTRP, where they connect each consecutive repeat (with the exception of the same three residues at the amino (N) terminus). The individual repeats are amphipathic, with the interfaces between α-helices composed largely of alanine, leucine and isoleucine residues, while the solvent-exposed surfaces of the same helices are composed largely of lysine and glutamate residues.

The construct names and sequences described in this paper, and a list of figures illustrating those constructs, are provided in Supplementary Table 1. Many constructs are referred to within the remainder of this article (and in that table) as '$cTRP24_x$', where the cTRP24 molecule is assembled from multiple, smaller, identical protein subunits, where each subunit contains 'x' repeats. For example, $cTRP24_6$ (read as, 'cTRP24 sub6') refers to a protein subunit containing six repeats, which tetramerizes to form a cTRP24 particle consisting of 24 total repeats. Some constructs contain disulfide staples between the protein subunits and are named $cTRP24_x$SS.

[1]Clinical Research Division, Fred Hutchinson Cancer Research Center, Seattle, WA, USA. [2]Division of Basic Sciences, Fred Hutchinson Cancer Research Center, Seattle, WA, USA. [3]Department of Biology, Seattle University, Seattle, WA, USA. [4]Program in Computational Biology, Public Health Sciences Division, Fred Hutchinson Cancer Research Center, Seattle, WA, USA. ✉e-mail: kaiserb@seattleu.edu; bstoddar@fredhutch.org; pbradley@fredhutch.org

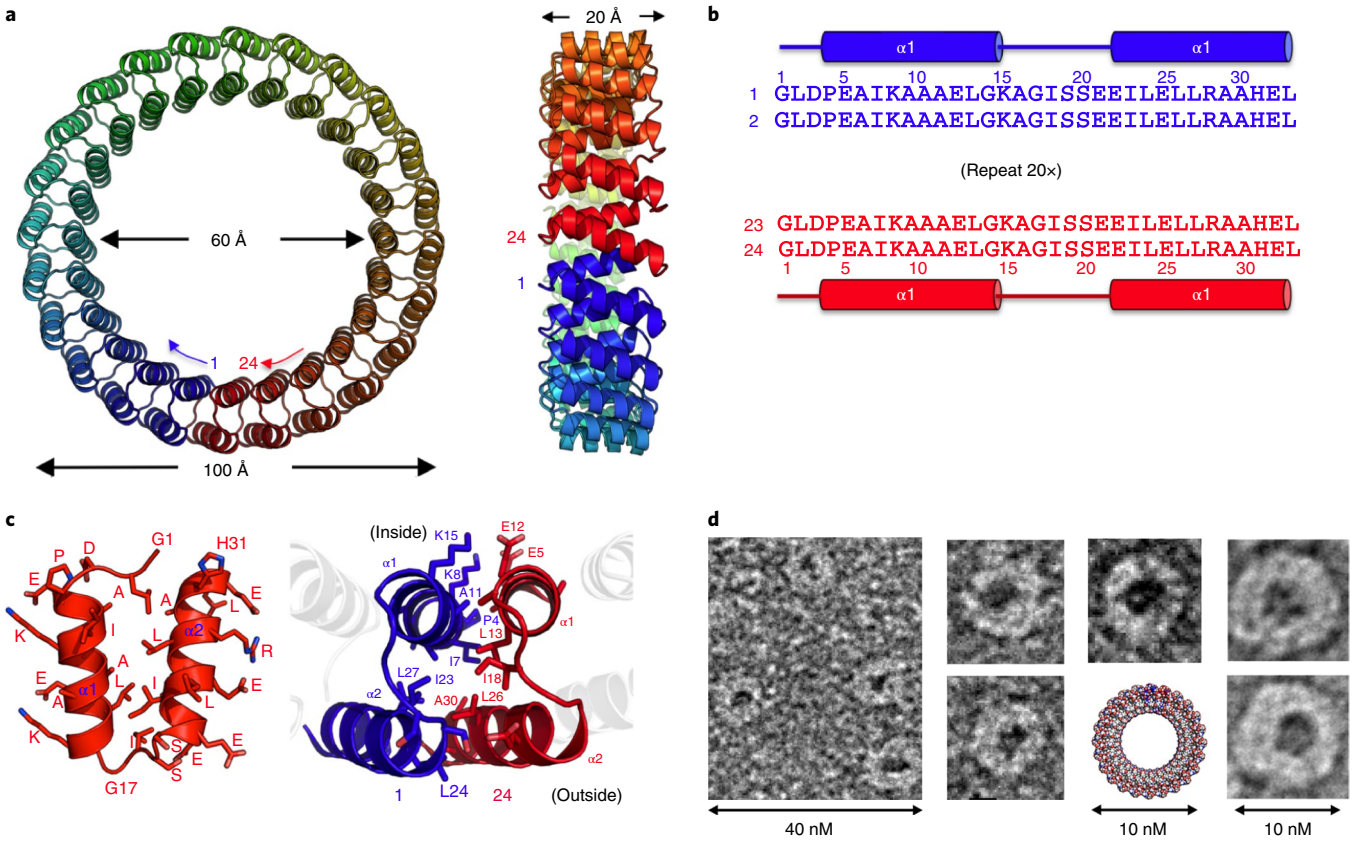

Fig. 1 | Properties of an engineered 24-repeat circular tandem repeat protein. a,**b**, Topology, dimensions (**a**), sequence and secondary structure content (**b**) of a computational model of the protein nanoparticle. The engineered construct (cTRP24) contains 24 repeated structural units (a left-handed two-helix bundle) corresponding to exact repeats of a 33-amino acid sequence. The interface between the N- and C-terminal repeats (no. 1 and no. 24) is identical to that between all other internal repeats. The outer diameter of the cTRP24 is ~100 Å, its width is ~20 Å and the inner diameter is ~60 Å. **c**, Computational model showing the fold and side chain distribution of a single structural repeat (left) and of the interface between two consecutive structural repeats (right). The inner and outer surfaces of the cTRP24 are primarily lined with pairs of lysine and glutamate residues. **d**, Negative-stain EM images of cTRP24. The dimensions and thickness of the observed nanoparticles are in close agreement with those corresponding to a space-filled model of the designed construct.

cTRP24 was expressed at high levels (>20 mg per liter of bacterial culture) and was easily concentrated to millimolar concentrations (50–100 mg ml^{-1}), with no evidence of aggregation or precipitation during concentration. The purified protein was examined using circular dichroism (CD) spectroscopy, small angle X-ray scattering (SAXS) and electron microscopy (EM). CD spectra (Extended Data Fig. 1a) confirmed the α-helical nature of the protein and retention of the folded structure up to 95 °C. SAXS spectra (Extended Data Fig. 1b) were closely superimposable on theoretical spectra calculated from designed coordinates of the cTRP (reproducible across a wide range of protein concentrations). Finally, the shape of the protein in the EM images (Fig. 1d) revealed uniform nanoparticles displaying circular shapes approximately 100 Å (10 nm) across their outer diameter, with obvious internal pores and overall thickness similar to the designed protein.

The protein was also crystallized; however, all specimens diffracted to very low resolution. We believe that result is due to very high solvent content (promoted in part by the large internal pores of the cTRP construct) and to rotational averaging of the symmetric molecule throughout the lattice.

Assembly from smaller subunits. The ultimate goal of this work was to display multiple copies of functional protein domains (that is, 'cargo') at symmetrically distributed positions around the cTRP periphery. To reduce the size and complexity of such constructs (and to generate constructs containing multiple termini for alternative fusion sites), we investigated assembly of the cTRP from smaller fragments. These constructs were each intended to assemble into a protein nanoparticle containing 24 total repeats (that is, constructs with 3, 4, 6, 8 or 12 repeats that might assemble into full-sized cTRPs via octamerization, hexamerization, tetramerization, trimerization or dimerization, respectively).

These constructs also expressed at very high levels, purified to homogeneity (Fig. 2a, inset) and behaved similarly in solution to full-length cTRP24. However, size-exclusion chromatography (SEC) analysis showed that the smallest four constructs eluted at volumes consistent with their monomeric size, indicating a failure to assemble into the desired 24-repeat construct. The largest of the constructs (cTRP24$_{12}$, which was expected to dimerize) coeluted at the same volume as the cTRP24 protein; however, a significant tail extending from the main peak indicated that the protein appeared to sample an equilibrium between dimers and monomers. Subsequent repeats of this experiment at various pH values ranging from 6.5 to 8.5 produced similar elution patterns (Fig. 2b).

We hypothesized that cTRP assembly might be encouraged by engineering disulfide bonds into the interfaces between protein subunits. We identified a pair of positions in the N- and carboxy (C)-terminal repeats of each subunit (proline 4 on the N-terminal repeat, and alanine 6 on the C-terminal repeat) that might

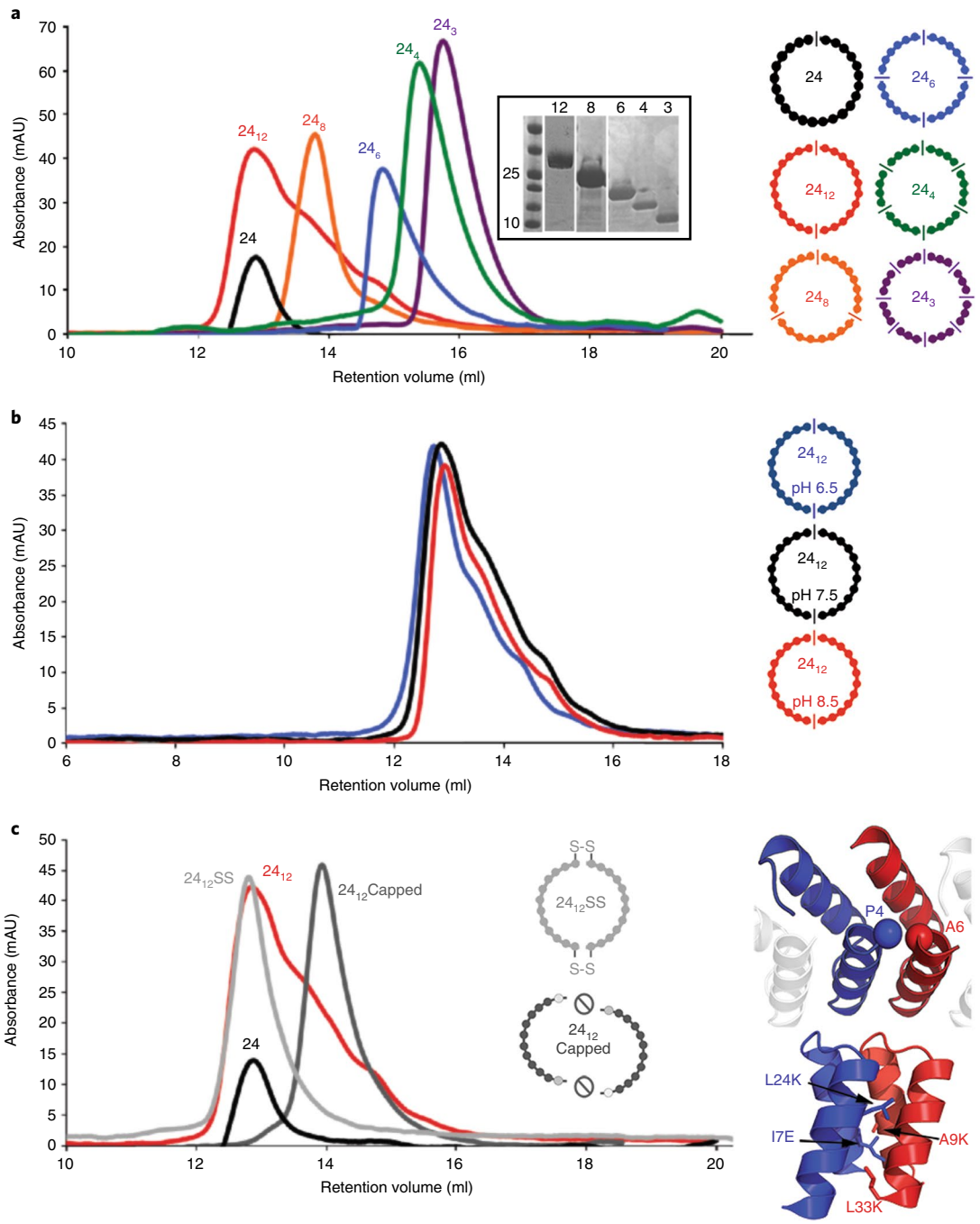

Fig. 2 | Assembly of cTRP24$_x$ nanoparticles from smaller protein subunits, verified by SEC analyses. a, Constructs containing 3, 4, 6, 8, 12 or 24 repeats were individually expressed and purified from *E. coli* using identical protocols (see Methods); each construct was run at concentrations of approximately 10 mg ml^{-1}. The elution profiles indicate that the smaller constructs (containing 3–8 repeats per subunit) fail to assemble into a full 24-repeat cTRP. The largest subunit (containing 12 repeats; cTRP24$_{12}$) migrates with the full-sized cTRP24, consistent with an intact dimer, but a long tail extending from the peak indicates that the construct is in dynamic equilibrium between dimeric and monomeric species (the latter probably sampling a range of conformations). **b**, Assembly behavior of cTRP24$_{12}$ construct as a function of pH. Between pH 6.5 and 8.5 the elution behavior of the construct appears to be largely unchanged. **c**, SEC analysis of a 12-repeat construct, with a pair of point mutations (P4C and A6C, shown in computational structural models on the right) introduced at the interface of the N- and C-terminal repeats creating a disulfide 'stapled' protein homodimer (cTRP24$_{12}$SS). The resulting construct eluted as a single symmetric peak at the same elution volume as the monomeric cTRP24 construct. SDS–PAGE analyses under reducing and nonreducing conditions also support formation of a disulfide-stapled dimer (Extended Data Fig. 2). An additional construct, harboring four mutations to physically prevent dimerization (cTRP24$_{12}$Capped), was used as a negative control for dimeric assembly.

support disulfide formation if mutated to cysteines (Fig. 2c, right). Generation of a construct containing 12 repeats with those substitutions (cTRP24$_{12}$SS), and subsequent electrophoretic analyses under reducing and nonreducing conditions, confirmed the formation of a disulfide-coupled construct (Extended Data Fig. 2a). SEC analyses (Fig. 2c) revealed that the stapled construct coelutes at the same volume as the full-length cTRP24 construct, but now as a much sharper peak corresponding to a uniform size distribution.

An additional negative control, in which the original 12-repeat construct was mutated to sterically block subunit association, resulted in elution at a significantly retarded volume corresponding to a smaller monomeric construct (Fig. 2c; cTRP24$_{12}$Capped).

We repeated the same experiments using subunits containing only six repeats per protein chain, which were expected to assemble into disulfide-stapled tetramers (cTRP24$_6$SS). When expressed in bacterial cells (Extended Data Fig. 2b, middle panel), the resulting protein displayed an SEC elution profile corresponding to a cTRP tetramer, but it contained an incomplete complement of internal disulfide bonds (indicated by a ladder of protein bands on nonreducing SDS–PAGE). In contrast, when expressed and secreted from human 293 cells (Extended Data Fig. 2b, right panel), the same nanoparticle displayed a uniform and complete complement of interchain disulfide bonds.

Display and characterization of functional protein domains. Armed with self-assembling cTRP constructs containing 24 repeats, we next investigated our ability to display multiple copies of functional protein domains at positions distributed evenly around the periphery of the cTRP. Each assembled cTRP contained four protein domains either fused to the N terminus of each subunit or inserted within four surface loops (Supplementary Table 1). These correspond to the following.

1. Constructs harboring either a sequence-specific SH2 peptide-binding domain[12] (Fig. 3a; cTRP24$_{12}$SS-SH2), or
2. a 'SpyCatcher' protein ligation domain[13] (Fig. 3b; cTRP24$_{12}$SS-Spy) inserted into loops distributed around the top surface of the cTRP. The construct with the SpyCatcher domains was subsequently used to capture 'SpyTagged' versions of the SH2 domain or the Clover fluorescent protein[14].
3. An engineered fluorescent protein (mFAP)[15] inserted in loops distributed around the bottom face of the cTRP (Extended Data Fig. 3c; cTRP24$_6$SS-mFAP).
4. A single-chain class I major histocompatibility complex molecule (scMHC, a construct consisting of an antigenic peptide, β_2-microglobulin and MHC heavy chain encoded on a single polypeptide[16]) fused to four equivalent N termini distributed around the cTRP tetramer (Fig. 4a and Extended Data Fig. 4; cTRP24$_6$SS-scMHC). This construct displays a viral antigen (CMV pp65 peptide from cytomegalovirus) and was created to demonstrate its performance as a highly avid staining reagent (for example, identification of T cells expressing receptors specific for that cognate MHC–peptide complex).
5. We also generated a hexameric form of the same CMV pp65 scMHC (Extended Data Fig. 5a; cTRP24$_4$SS-scMHC) further demonstrating the flexibility of the cTRP24 platform.
6. Four copies each of two distinct protein domains, each fused to opposite faces of the cTRP protein scaffold (Extended Data Fig. 5b), by combining the protein domains found in (3) and (4) above.
7. A single-chain Fv targeting the T-cell coreceptor CD28 fused to the four N termini within the cTRP24$_6$SS scaffold, for use in T-cell activation and expansion assays (Fig. 5; cTRP24$_6$SS-scFv^{CD28}).
8. Three separate single-chain tumor necrosis factor receptor superfamily ligand trimers (each generated for this project; see Methods) that, respectively, target T-cell coreceptors 4-1BB, OX40 and CD27, each fused to the four N termini of the cTRP24$_6$SS scaffold (Fig. 6; cTRP24$_6$SS-scTrimer^{Ligand}).

The expression, purification and assembly of all these constructs were confirmed by gel electrophoresis and SEC, and the tetrameric organization and geometry of the functionalized cTRP24$_6$SS nanoparticle containing four copies of the scMHC were further visualized via EM microscopy (Fig. 4b).

We first examined the behavior of the two constructs containing either an SH2 domain (which binds a phosphotyrosyl-containing peptide EHIpYDEVAAD)[12] or a SpyCatcher protein ligation domain (which captures protein domains fused to an N-terminal 'SpyTag' peptide sequence)[13] (Fig. 3). Initial tests of the protein ligation function of the cTRP24$_{12}$SS-Spy fusion protein via incubation with a 'SpyTagged' Nck2 SH2 domain demonstrated that the SpyCatcher domains could be fully conjugated with the cargo protein in a 15-min incubation at room temperature (Fig. 3c; far right), similar to the kinetics reported for the free SpyCatcher domain[13]. To further test the SpyCatcher domain, we covalently coupled cTRP24$_{12}$SS-Spy to four copies of SpyTagged 'Clover'[14] (Extended Data Fig. 3a,b).

Next, we examined SH2-dependent phosphopeptide binding by four constructs: the cTRP24$_{12}$SS scaffold, the free SH2 domain, cTRP24$_{12}$SS-SH2 and cTRP24$_{12}$SS-Spy ligated to four copies of SpyTag-SH2 (cTRP24$_{12}$SS-Spy-SH2). The experiments were performed in solution (using fluorescence polarization with a labeled peptide ligand) and on a surface (using surface plasmon resonance (SPR), with biotin-labeled peptide captured on a streptavidin chip). In the solution-based peptide-binding experiment (Fig. 3d), the constructs were all observed to bind peptide in a saturable manner, with approximate K_d values of 200–500 nM, which is similar to previously reported values for the same SH2/peptide combination[12]. The cTRP24$_{12}$SS scaffold alone did not display significant peptide binding.

In surface-based binding experiments against the same peptide target, superimposable binding kinetics were observed for both the cTRP24$_{12}$SS-SH2 and cTRP24$_{12}$SS-Spy-SH2 fusions (Fig. 3e). Both constructs display a significant avidity effect, primarily manifested in a considerably slower off-rate. This difference in off-rates between free SH2 domains versus a cTRP array of SH2 domains increases significantly when capturing a high density of peptide on the chip (data not shown).

We also tested incorporation of cTRP nanoparticles with functional cargo fused to multiple positions around the opposite ('bottom') face by inserting copies of a de novo-engineered fluorescence-activating protein[7] (mFAP) into four evenly spaced loops (Extended Data Fig. 3c,d; cTRP24$_6$SS-mFAP). The cTRP24$_6$SS-mFAP protein also expressed at very high levels, displayed excellent solution properties upon purification and exhibited similar fluorescent properties when compared to free mFAP[15].

Display and characterization of eukaryotic protein constructs. While the constructs described above all folded and expressed well in *Escherichia coli*, many secreted eukaryotic proteins that are of interest cannot be generated in bacteria. We therefore adapted the cTRP platform for use in mammalian expression systems and tested the production and function of various mammalian secretory proteins. As an initial proof-of-concept, we fused four copies of an scMHC to the cTRP24$_6$ and cTRP24$_6$SS scaffolds in an attempt to provide an alternative route to streptavidin-based tetramers, which are typically refolded from bacterial inclusion bodies (Fig. 4a). The constructs were secreted from 293F cells using a previously described lentiviral-based protein expression system[17]. Expression of cTRP24$_6$SS-scMHC resulted in an approximate yield of 100 mg l^{-1} of conditioned media; subsequent purification yielded a fully assembled tetramer (Fig. 4b,c) containing disulfide bonds that could be reduced to generate a shift in electrophoretic mobility (Fig. 4c). In contrast, the cTRP24$_6$-scMHC construct lacking the engineered disulfide bonds ran as an unassembled monomer.

The functional activity of the resulting constructs was tested in a flow cytometry assay in which a CMV-reactive cytotoxic T-cell line (CTL) or healthy CMV-negative donor peripheral blood mononuclear cells (PBMCs) were stained with the cTRP24$_6$-scMHC monomer or the cTRP24$_6$SS-scMHC tetramer using a fluorophore-labeled anti-His antibody as a secondary detection reagent (Fig. 4d). This experiment demonstrated that (1) the unassembled

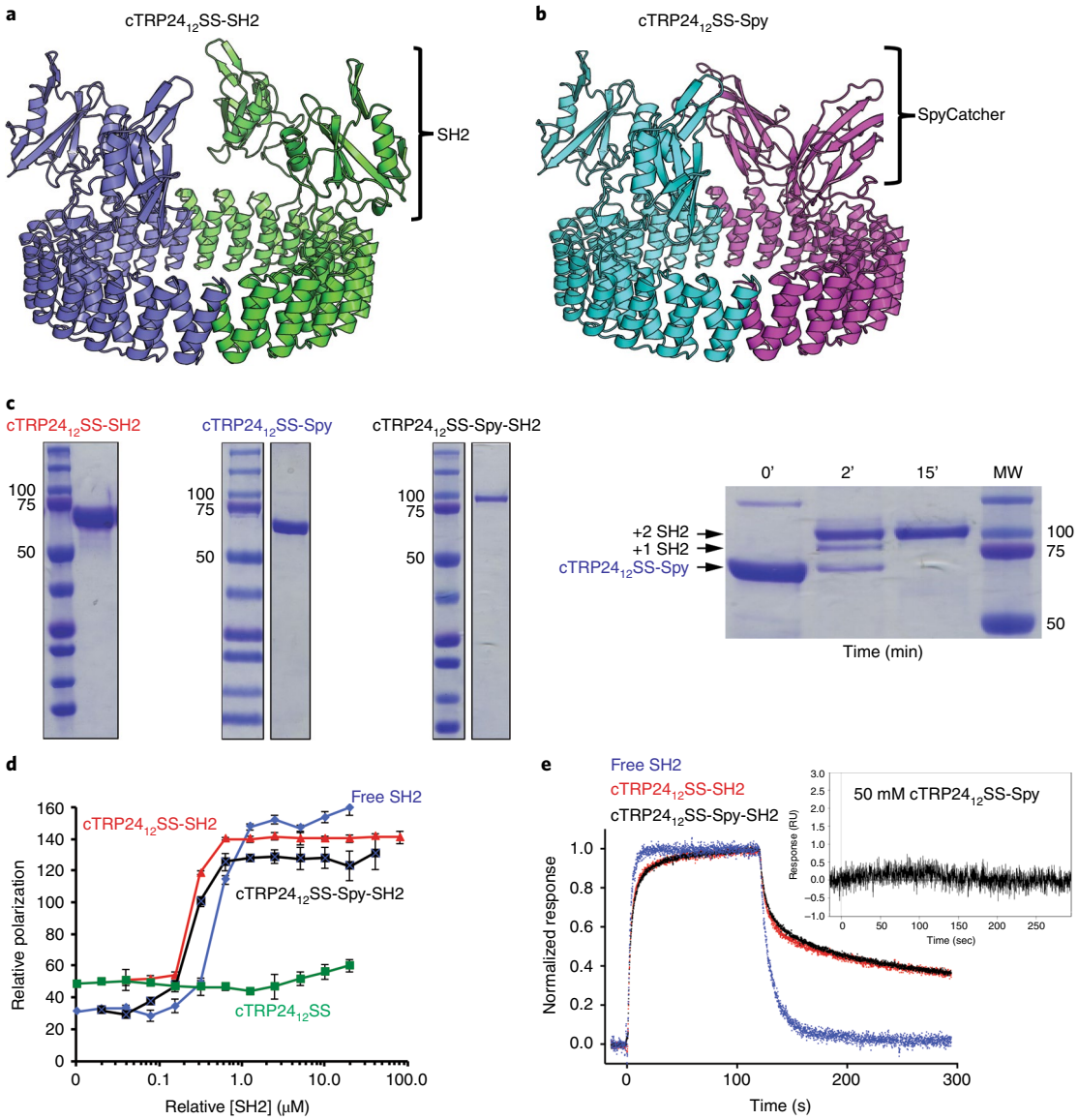

Fig. 3 | Computational models and characterization of functionalized 24-repeat cTRP constructs. a,**b**, The sequence-specific peptide-binding SH2 domain and the SpyCatcher ligation domain are modeled into four evenly distributed loops around the top face of the cTRP (cTRP24$_{12}$SS-SH2 (**a**); cTRP24$_{12}$SS-Spy (**b**)). Ribbon diagrams represent models of designed constructs. **c**, Reducing SDS–PAGE analyses of cTRP24$_{12}$SS-SH2, cTRP24$_{12}$SS-Spy and cTRP24$_{12}$SS-Spy that has been conjugated with four copies of a SpyTagged SH2 domain (cTRP24$_{12}$SS-Spy-SH2) (left). Demonstration of covalent ligation of SpyTag-SH2 to the cTRP24$_{12}$SS-Spy construct (right). Ligation proceeds to completion within 15 min at room temperature. **d**, Peptide binding in solution by free SH2 and by cTRP24$_{12}$SS-SH2 domains. Fluorescence polarization (FP) with labeled Tir10 phosphotyrosyl peptide (corresponding to the physiological binding target for the Lck SH2 domain) was performed using purified free SH2 domain (blue), cTRP24$_{12}$SS-SH2 (red) and cTRP24$_{12}$SS-Spy-SH2 (black). A control experiment was also conducted using the free cTRP24$_{12}$SS nanoparticle (green) harboring no functional protein domains. The protein concentration is normalized to account for the 4:1 ratio of SH2 domains per molecule (four per cTRP; one per free SH2). All three constructs display saturable binding and an approximate K_d of 200–300 nM. All binding experiments were conducted in triplicate using independent aliquots of each protein. Data shown as mean and s.d. for $n = 3$ measurements using independent protein aliquots; source data are available online. **e**, Free SH2, cTRP24$_{12}$SS-SH2 and cTRP24$_{12}$SS-Spy-SH2 binding to surface-bound peptide. SPR was used to measure the binding of purified free SH2 domain (blue), cTRP24$_{12}$SS-SH2 (red) and cTRP24$_{12}$SS-Spy-SH2 (black) to immobilized biotinylated phosphotyrosyl peptide. A cTRP24$_{12}$SS-Spy construct without SH2 domains did not display measurable peptide binding (inset).

cTRP24$_6$-scMHC monomer insufficiently stained the CMV-reactive CTL clone, and that (2) the avidity gained from tetramerization of the scMHC construct rescued target-specific staining.

In a parallel experiment (Extended Data Fig. 4), the same CTLs were serially diluted into freshly thawed PBMCs and detected using either the cTRP24$_6$SS-scMHC (along with the secondary detection antibody) or a classical streptavidin-conjugated tetramer of the same scMHC construct (used as a positive control). This experiment demonstrated that the limits of detection of the cTRP24$_6$SS-scMHC and classical streptavidin-conjugated tetramer are comparable, despite the technical differences between the two approaches.

To further demonstrate the utility of self-assembling cTRPs, we next designed a series of T-cell 'superagonists' that could potentially be used as soluble protein reagents to mimic immunological synapse interactions in vitro, which are important during the

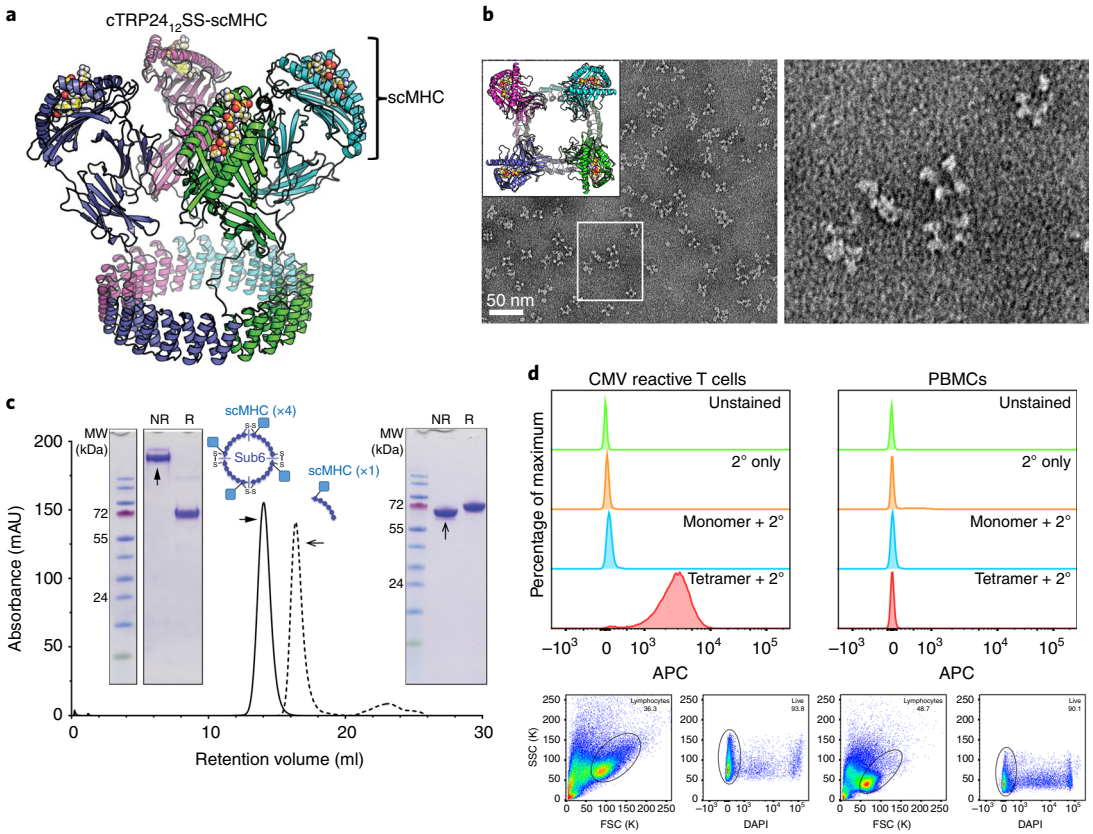

Fig. 4 | Characterization of an scMHC tetramer expressed and purified from human 293 cells. a, Ribbon diagram of a computational model showing the structure of cTRP24$_6$SS-scMHC, with antigenic peptide rendered as spheres. The construct is composed of a disulfide-stapled tetramer, wherein each subunit consists of an N-terminal single-chain MHC trimer (scMHC) fused to six cTRP repeats. **b**, Negative-stain EM images of a field of cTRP24$_6$SS-scMHC particles. The fourfold symmetric arrangement of the scMHC domains around each particle, many of which are oriented with the cTRP in the plane of the grid, is clearly visible. Top view of the model in panel **a** (inset). **c**, Nonreducing (NR) and reducing (R) SDS–PAGE and SEC analyses of disulfide-stapled, tetrameric cTRP24$_6$SS-scMHC (left, gel inset and solid elution trace) and unstapled, monomeric cTRP24$_6$-scMHC (right, gel inset and dashed elution trace). The change in mobility under reducing conditions is due to the dissolution of the tetrameric assemblage and/or loss of disulfides in the scMHC cargo for the two respective constructs. **d**, Flow cytometry analyses of T-cell staining with cTRP24$_6$-scMHC monomer and cTRP24$_6$SS-scMHC tetramer. A CMV pp65-reactive CD8$^+$ T-cell line was stained (left histogram) with monomeric or tetrameric constructs using a secondary (2°) anti-His-iFluor647 antibody. Also shown are histograms for unstained cells and anti-His-iFluor647 stained cell as controls. While the monomeric cTRP produces a negligible fluorescent staining signal, the tetrameric construct labels close to 100% of the cells. Background staining (right histogram) was assessed using PBMCs isolated from a CMV$^-$ donor using identical staining conditions. Offset histograms were gated from lymphocyte (forward scatter (FSC)-side scatter (SSC)) and live cell (4,6-diamidino-2-phenylindole; DAPI$^-$) populations as indicated (bottom scatter plots).

process of T-cell differentiation and expansion[18]. Several agonistic antibodies exist against a variety of human T-cell costimulatory receptors (examples include the anti-CD28 antibody TGN1412 (theralizumab), anti-CD27 antibody 1F5 (varlilumab) and anti-CD3 antibody OKT3 (muromonab)). Bivalent reagents often work poorly in solution and, as a result, are often conjugated to beads (for example, Dynabeads Human T-Activator CD3/CD28) or aggregated on tissue culture plates to drive robust T-cell expansion. Soluble, multimeric proteins that agonize costimulatory receptors and thereby induce canonical signaling pathways could serve as an alternative to typical culture systems, especially if they could: (1) be easily expressed and purified, (2) be added directly to tissue culture medium at low concentrations, (3) be easily washed away or inactivated and (4) enable large-scale suspension or bioreactor expansion of human T cells.

To investigate this idea, we first designed a CD28 agonist (cTRP24$_6$SS-scFv^{CD28}) using the variable region (as a single-chain Fv) of the CD28-specific antibody TGN1412. The scFv was successfully displayed in a tetrameric arrangement and easily purified from conditioned media (Fig. 5a). The functionality of the molecule was verified using an NF-κB Jurkat reporter line in the presence of plate-immobilized OKT3 (Fig. 5b). We next assessed proliferation capacity of carboxyfluorescein succinimidyl ester (CFSE)-labeled human CD8$^+$ T cells in vitro. The addition of soluble cTRP24$_6$SS-scFv^{CD28} enhanced OKT3-induced proliferation to a similar extent to the soluble superagonistic TGN1412 monoclonal antibody (Fig. 5c). These combined results show that cTRP24$_6$SS-scFv^{CD28} is active when combined with OKT3, and demonstrate that displaying scFvs as cTRP24 multimeric arrangements could be a robust way to generate soluble receptor agonists.

Finally, we designed and expressed a series of TNF receptor superfamily ligands (4-1BBL, OX40L and CD70) as single-chain fusions to the cTRP24$_6$SS scaffold, to generate a toolkit of T-cell superagonists (Fig. 6a,b). Each of these tetramers secreted well from 293F cells and ran as monodispersed, tetrameric proteins by SEC (Fig. 6b). The functionality of the cTRP24$_6$SS-scTrimer^{CD70} (Fig. 6b, inset shows SDS–PAGE) was confirmed using a CFSE-based T-cell proliferation assay. The addition of soluble cTRP24$_6$SS-scTrimer^{CD70} increased OKT3-induced proliferation of CD8$^+$ T cells in vitro (Fig. 6c). Furthermore, the binding capacity of the

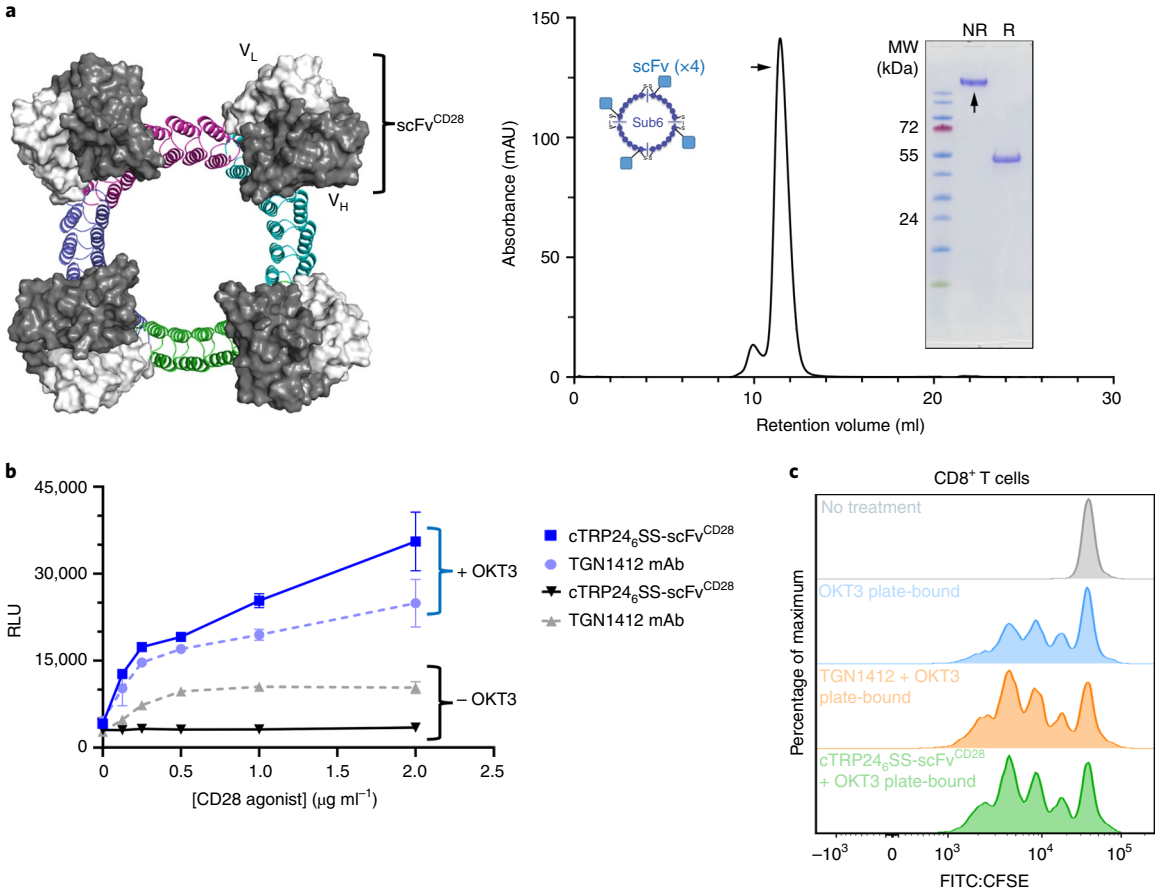

Fig. 5 | Functional characterization of a cTRP24$_6$SS construct harboring an N-terminal single-chain Fv (scFv) specific for the T-cell costimulatory receptor CD28. a, Structural diagram showing top-down view of the designed cTRP24$_6$SS-scFv^{CD28} construct (left). The properly assembled, disulfide-stapled construct displays four copies of the scFv region of an anti-CD28 antibody (derived from TGN1412). The scFv is rendered as a gray and white space-filling model; heavy chain variable (V_H) and light chain variable (V_L) regions are indicated. SEC and SDS–PAGE analyses of purified cTRP24$_6$SS-scFv^{CD28} expressed in human 293 cells indicate proper assembly of the tetrameric construct (right). SEC was performed on a Superose 6 10/300 GL (GE) column and SDS–PAGE was performed under nonreducing (NR) and reducing (R) conditions. **b**, Jurkat T-cell activation assay using anti-CD3 and anti-CD28 agonists. Jurkat T cells expressing an NF-κB luciferase reporter for T-cell activation were incubated with soluble cTRP24$_6$SS-scFv^{CD28} or the superagonistic monoclonal antibody TGN1412 in the presence or absence of plate-bound anti-CD3 OKT3. In the presence of OKT3, cTRP24$_6$SS-scFv^{CD28} efficiently induced T-cell activation. Data shown as mean and s.d. for $n = 2$ independent experiments; source data are available online. **c**, A CFSE-based T-cell expansion assay. CFSE dilution as a function of human CD8$^+$ T-cell proliferation using plate-bound OKT3 (blue, 5 μg ml^{-1}) alone and in combination with soluble anti-CD28 superagonists TGN1412 (orange, 1 μg ml^{-1}) or cTRP24$_6$SS-scFv^{CD28} (green, 1 μg ml^{-1}). Nonactivated CD8$^+$ T cells were considered as CFSE^{hi} nonproliferating controls (gray).

OX40L and 4-1BBL tetramers was assessed using CD3/CD28-bead activated CD8$^+$ T cells at 4 d following activation. Incubation of CD8$^+$ T cells with cTRP24$_6$SS-scFv^{OX40L} and fluorophore-labeled anti-His antibody revealed similar OX40 receptor expression as compared to that via anti-OX40 monoclonal antibody (Fig. 6d). Similar results were observed for cTRP24$_6$SS-scFv$^{4\text{-}1BBL}$ (Extended Data Fig. 6). In summary, we document here that costimulatory receptors, such as CD28, CD27, OX40 and 4-1BB, can be effectively bound and triggered by soluble self-assembling cTRP24$_6$SS-ligand-expressing superagonists.

Discussion

The experiments described here demonstrate that a computationally designed cTRP scaffold is capable of displaying a wide variety of functional protein domains and of robust self-assembly from smaller repeating elements. The constructs display architectures that closely resemble their computational designs, are very soluble and thermostable and provide display platforms that facilitate arrangements of functional cargo that benefit from symmetric preorganization and significantly enhanced avidity. Such constructs may offer a straightforward approach for the development and application of a wide variety of platforms for use in biotechnological and industrial processes.

The ability of the cTRP scaffold to be assembled from smaller protein subunits, and to harbor functional protein domains through fusions at the N or C termini of each subunit and within individual surface loops, provides considerable flexibility in the design of functionalized constructs that are tailored to their folded structure. Additionally, the ability of the cTRP scaffold to be expressed and secreted at high levels from a eukaryotic (in this case, human) expression platform enables the creation of nanoparticles containing functional protein constructs that cannot typically be produced in prokaryotic systems.

Several areas of investigation and further development of engineered protein display systems, such as the cTRP constructs described in this study, seem apparent. These include sampling a variety of display symmetries (that is, two-, three-, four-, six- and/or eightfold distribution), the design of self-assembling particles that

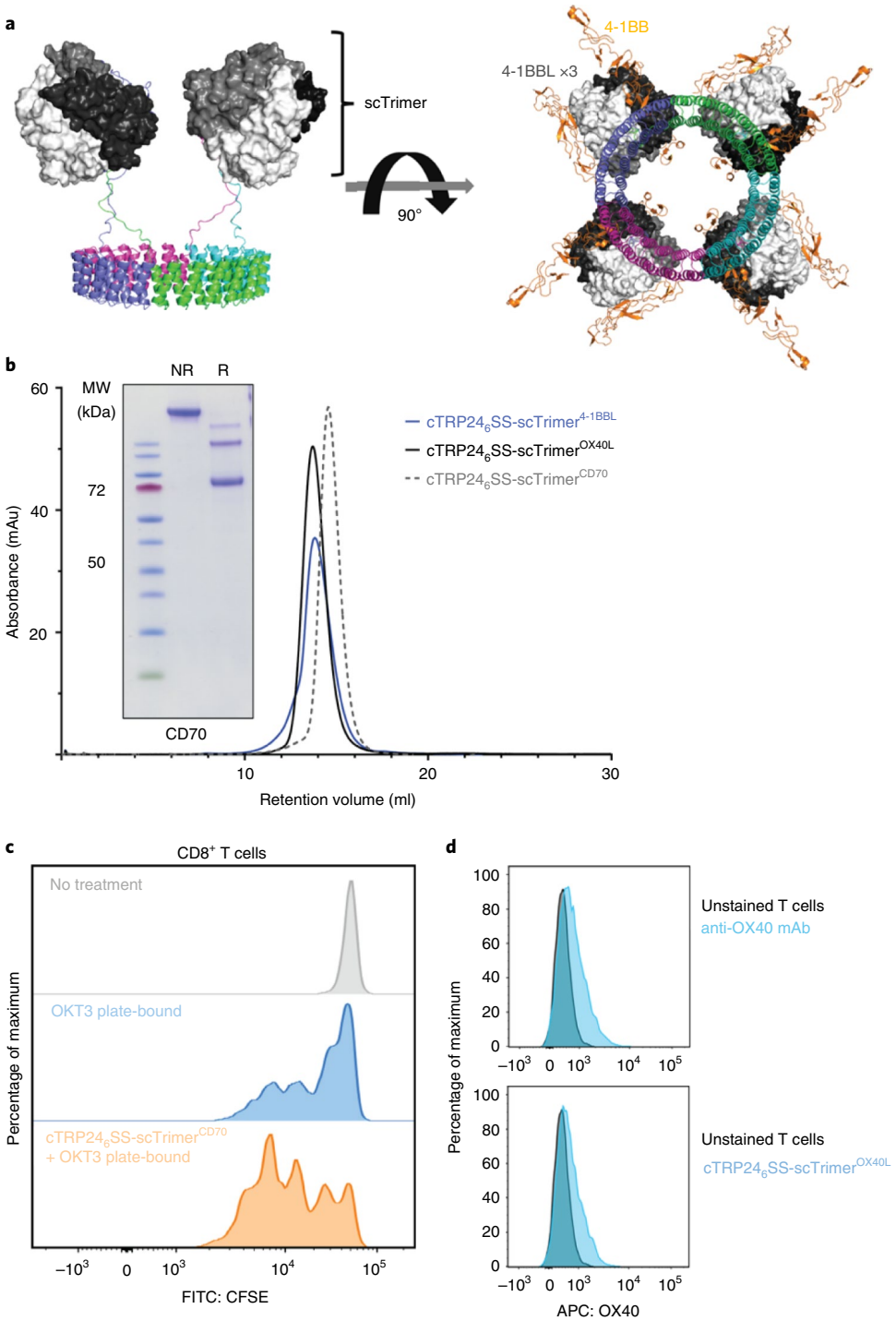

Fig. 6 | Functional characterization of cTRP24$_6$SS constructs harboring single-chain trimers of tumor necrosis factor receptor ligands targeting T-cell costimulatory receptors 4-1BB, OX40 and CD27. a, Structural diagram showing side view of the cTRP24$_6$SS-scTrimer$^{4\text{-}1BB}$, with the single-chain trimer rendered in space fill (left). Structural model (looking down at the T-cell surface) showing theoretical 4-1BB receptor clustering in which the nanoparticle simultaneously engages up to 12 individual receptors (right). 4-1BB and 4-1BBL complex structures were built using PDB 6A3V. **b**, SEC analyses of all three tetramers. Inset shows SDS–PAGE gel of cTRP24$_6$SS-scTrimer^{CD70}. **c**, CFSE dilution assay of activated human CD8$^+$ T cells using plate-bound OKT3 (blue, 5 µg ml^{-1}) alone and in combination with soluble cTRP24$_6$SS-scTrimer^{CD70} (orange, 1 µg ml^{-1}). Nonactivated CD8$^+$ T cells were considered as CFSE^{hi} nonproliferating controls (gray). **d**, Surface expression of OX40 receptor as determined by antibody and cTRP tetramer staining. Staining of activated CD8$^+$ T cells (4 d poststimulation with anti-CD3/anti-CD28 beads) using an APC-labeled anti-OX40 (top) and cTRP24$_6$SS-scTrimer^{OX40L} using a secondary anti-His-iFluor647 (bottom). Unstained controls are shown (black). Detection of 4-1BB on activated T cells is shown using cTRP24$_6$SS-scTrimer$^{4\text{-}1BBL}$ in Extended Data Fig. 6.

form obligate heterodimers or other multimers (thereby facilitating the introduction of defined ratios of different cargo molecules across the surface of the construct), the introduction of a wider variety of functional protein cargoes that might benefit from symmetric preorganization and avidity (such as receptor ligands or ectodomains, antibody domains or enzymatic catalysts) and the

design of thicker cTRP structures (perhaps facilitating the creation of artificial transmembrane structures or nanodiscs).

Online content

Any methods, additional references, Nature Research reporting summaries, source data, extended data, supplementary information, acknowledgements, peer review information; details of author contributions and competing interests; and statements of data and code availability are available at https://doi.org/10.1038/s41594-020-0397-5.

Received: 24 January 2020; Accepted: 13 February 2020;
Published online: 23 March 2020

References

1. Itzhaki, L. S. & Lowe, A. R. From artificial antibodies to nanosprings: the biophysical properties of repeat proteins. *Adv. Exp. Med. Biol.* **747**, 153–166 (2012).
2. Matsushima, N., Tanaka, T. & Kretsinger, R. H. Non-globular structures of tandem repeats in proteins. *Protein Pept. Lett.* **16**, 1297–1322 (2009).
3. Javadi, Y. & Itzhaki, L. S. Tandem-repeat proteins: regularity plus modularity equals design-ability. *Curr. Opin. Struct. Biol.* **23**, 622–631 (2013).
4. Schilling, J., Schoppe, J. & Pluckthun, A. From DARPins to LoopDARPins: novel LoopDARPin design allows the selection of low picomolar binders in a single round of ribosome display. *J. Mol. Biol.* **426**, 691–721 (2014).
5. Zhao, Y.-Y. et al. Expanding RNA binding specificity and affinity of engineered PUF domains. *Nucleic Acids Res.* **46**, 4771–4782 (2018).
6. Cunha, E. S., Hatem, C. L. & Barrick, D. Insertion of endocellulase catalytic domains into thermostable consensus ankyrin scaffolds: effects on stability and cellulolytic activity. *Appl. Environ. Microbiol.* **79**, 6684–6696 (2013).
7. Park, K. et al. Control of repeat-protein curvature by computational protein design. *Nat. Struct. Mol. Biol.* **22**, 167–174 (2015).
8. Cheng, C. Y., Jarymowycz, V. A., Cortajarena, A. L., Regan, L. & Stone, M. J. Repeat motions and backbone flexibility in designed proteins with different numbers of identical consensus tetratricopeptide repeats. *Biochemistry* **45**, 12175–12183 (2006).
9. Kajander, T., Cortajarena, A. L., Mochrie, S. & Regan, L. Structure and stability of designed TPR protein superhelices: unusual crystal packing and implications for natural TPR proteins. *Acta Crystallogr. D Biol. Crystallogr.* **63**, 800–811 (2007).
10. Shen, H. et al. De novo design of self-assembling helical protein filaments. *Science* **362**, 705–709 (2018).
11. Doyle, L. et al. Rational design of alpha-helical tandem repeat proteins with closed architectures. *Nature* **528**, 585–588 (2015).
12. Frese, S. et al. The phosphotyrosine peptide binding specificity of Nck1 and Nck2 Src homology 2 domains. *J. Biol. Chem.* **281**, 18236–18245 (2006).
13. Zakeri, B. et al. Peptide tag forming a rapid covalent bond to a protein, through engineering a bacterial adhesin. *Proc. Natl Acad. Sci. USA* **109**, E690–E697 (2012).
14. Lam, A. J. et al. Improving FRET dynamic range with bright green and red fluorescent proteins. *Nat. Methods* **9**, 1005–1012 (2012).
15. Dou, J. et al. De novo design of a fluorescence-activating beta-barrel. *Nature* **561**, 485–491 (2018).
16. Yu, Y. Y., Netuschil, N., Lybarger, L., Connolly, J. M. & Hansen, T. H. Cutting edge: single-chain trimers of MHC class I molecules form stable structures that potently stimulate antigen-specific T cells and B cells. *J. Immunol.* **168**, 3145–3149 (2002).
17. Bandaranayake, A. D. et al. Daedalus: a robust, turnkey platform for rapid production of decigram quantities of active recombinant proteins in human cell lines using novel lentiviral vectors. *Nucleic Acids Res.* **31**, e143 (2011).
18. Chen, L. & Flies, D. B. Molecular mechanisms of T cell co-stimulation and co-inhibition. *Nat. Rev. Immunol.* **13**, 227–242 (2013).

Methods

Computational design. The 24-repeat cTRP scaffold was designed using a modified version of the tandem repeat protein design protocol introduced in Doyle et al.[11]. This protocol consists of an initial large-scale exploration of cTRP topologies (helix lengths and turn types) compatible with the desired repeat number, followed by a round of focused design simulations targeting a handful of specific topologies. In the first stage we explored helix lengths compatible with a total repeat length between 30 and 40 residues. In the second stage we focused on two specific topologies (with inner/outer helix lengths of 13/14 and 14/11, respectively) that emerged as consensus low-energy solutions. Of the order of 100,000 design simulations were conducted in each stage, with each independent run consisting of a fragment-based backbone buildup, followed by all-atom sequence design and structure relaxation. On the basis of the observation of overpacking in our previously published designs, we modified the all-atom sequence design calculation to penalize close contacts more stringently. Final designs were selected on the basis of the ability of structure prediction simulations to recapitulate the designed structure when given only the designed sequence, with a final manual inspection to assess surface composition, buried unsatisfied polar residues and packing quality.

Protein expression and purification from *E. coli*. The SH2 domain of human Nck2 cloned into pGEX-6P1 (ref. [12]) was a gift from T. Stradal (Helmholtz Centre for Infection Research). SH2 was amplified by PCR, with primers adding NcoI and NotI sites at the 5′ and 3′ ends of DNA, and subcloned into linearized pET15HE[19] using the NEBuilder HiFi DNA Assembly Kit (New England Biolabs). All other genes were synthesized commercially and subcloned into the same pET15HE bacterial expression vector (GenScript).

Plasmids were transformed into BL21(DE3)-RIL *E. coli* cells (Agilent Technologies) and plated on LB medium with ampicillin (100 μg ml^{-1}). A 10-ml aliquot of LB-ampicillin media was inoculated with a single colony and shaken overnight at 37 °C. Overnight cell cultures were added to 1-l volumes of LB-ampicillin, which were then shaken at 37 °C until the cells reached an optical density of 0.6–0.8 at 600 nm. The cells were chilled for 20 min at 4 °C, and IPTG was added to a final concentration of 0.3 mM to induce protein expression. The cultures were shaken overnight at 16 °C, and then pelleted by centrifugation and stored at −20 °C until purification.

For protein constructs without disulfide staples and for the free SH2 domain, cell pellets from 1 l of cell culture were resuspended in 50 ml of purification buffer (PBS with 20 mM imidazole pH 8.0). Cells were lysed via sonication and centrifuged to remove cell debris. The supernatant was passed through a 5-μm filter, and then incubated on a rocker platform at 4 °C for 1 h with 1 ml of nickel-NTA affinity resin (Invitrogen) equilibrated with purification buffer. After loading onto a gravity-fed column, the resin was washed three times with 10 ml of purification buffer, and the protein was eluted from the column by 10-min incubations with three consecutive aliquots of 5 ml of elution buffer (PBS with 300 mM imidazole pH 8.0). Fractions containing the eluted protein were pooled, filtered and run over SEC (BioRad ENrich 650) in PBS.

For protein constructs containing disulfide staples, cell pellets from 1 l of cell culture were resuspended in 50 ml of purification buffer (400 mM NaCl, 25 mM Tris pH 7.5, 20 mM imidazole pH 8.0). Cells were lysed via sonication and centrifuged to remove cell debris. The supernatant was passed through a 5-μm filter, and then incubated on a rocker platform at 4 °C for 1 h after adding 1 ml of nickel-NTA metal affinity resin (Invitrogen) equilibrated with purification buffer. After loading onto a gravity-fed column, the resin was washed eight times with 10 ml of purification buffer, and the protein was eluted from the column by 10-min incubations with three consecutive aliquots of 1.5 ml of elution buffer (300 mM NaCl, 25 mM Tris pH 7.5, 200 mM imidazole pH 8.0). Fractions containing the eluted protein were pooled and DTT was added to 5 mM. Pooled fractions were run over a HiTrap Q column (GE Healthcare) at 2 ml min^{-1} with a gradient from buffer A (25 mM Tris pH 7.5, 5 mM DTT) + 20% buffer B (25 mM Tris pH 7.5, 1 M NaCl, 5 mM DTT) to 100% buffer B over 20 ml. Fractions containing eluted protein were pooled, filtered and run over an SEC column (BioRad ENrich 650) in 150 mM NaCl, 25 mM Tris pH 7.5.

Protein expression and purification from human 293 cells. We employed the 'Daedalus' human cell line expression platform for the production and purification of secreted cTRP proteins, using methods described previously[17]. The expression system makes use of suspension-adapted HEK293 Freestyle cells and a highly optimized lentiviral transduction protocol to generate cell lines that secrete proteins at high levels. The lentiviral vector contains a *cis*-linked fluorescent protein reporter driven by an internal ribosome entry site that allows for tracking of relative protein expression levels. All mammalian proteins described in Supplementary Table 1 were purified directly from conditioned media using HisTrap FF Crude columns (GE, catalog no. 17528601) and subsequently polished on a Superose 6 10/300 GL SEC column (GE, catalog no. 17517201) using an AKTA pure 25 instrument.

CD spectroscopy. Purified recombinant protein was diluted to 10–20 μM and dialyzed overnight into 10 mM potassium phosphate buffer at pH 8.0. CD thermal denaturation experiments were performed on a JASCO J-815 CD spectrometer with a Peltier thermostat. Wavelength scans (190–250 nm) were carried out for each construct at 20 °C and 95 °C.

SAXS. Proteins were filtered and run over SEC (BioRad ENrich 650) in 150 mM NaCl, 50 mM Tris pH 7.5, 2% glycerol. Fractions containing pure protein were concentrated to a low and high range (about 2 mg ml^{-1} and 10 mg ml^{-1}, respectively) before being collected and averaged on the SIBLYS Beamline at the Advanced Light Source, Lawrence Berkeley National Laboratory[20]. FoXS was used to compare the fits to Rosetta-generated structures (https://www.rosettacommons.org/software).

Negative-stain EM analysis. Negative-stained specimens for transmission electron microscopy (TEM) were prepared using methods previously described[21]. Briefly, 4 μl of a cTRP solution at ~40–50 nM was applied to the surface of a freshly glow-discharged carbon film coated copper grid held at the tip of an anticapillary tweezer. The solution was adsorbed for 15–60 s. The grid was then washed three times by touching the surface to a 20-μl water droplet on the surface of a parafilm strip. Each time, the water attached to the grid was removed by briefly touching the surface of a nearby filter paper. The washing process was repeated twice with 20 μl and 40 μl of 0.7% uranyl formate (UF). The last droplet of UF was allowed to remain in contact with the grid for 15–60 s before removing the filter paper. The stained grid was air-dried for 5 min before storage in a grid box. Grids were analyzed by TEM using a Jeol1400 microscope operating at 120 kV. The images were recorded using a Gatan CCD detector at a nominal magnification of ×60,000 at the surface of the fluorescent screen.

Solution-binding analyses via fluorescence polarization. A ten-residue peptide, Tir10, containing a phosphorylated tyrosine (pY) was chemically synthesized with an fluorescein isothiocyanate (FITC) tag at the 5′ end linked to the peptide with a seven-atom aminohexanoyl spacer, Ahx (GenScript).

$$\text{Tir10}: \text{FITC} - \text{Ahx} - \text{EHI} - \text{pY} - \text{DEVAAD}$$

Tir10 stock was resuspended to 5.7 mM in DMSO, then diluted to 0.5 μM in fluorescence polarization (FP) buffer (20 mM HEPES, 150 mM KCl, pH 7.4). Proteins were exchanged into FP buffer then serially diluted twofold from 23 μM to 0.011 μM. Diluted proteins were mixed with Tir10 at a ratio of 9:1 for final concentrations of 20.7–0.01 μM protein and 0.05 μM Tir10. Mixtures were shielded from light and incubated at room temperature for 20 min. FP values were read at excitation of 485 nm and emission of 525 nm (SpectraMax M5). After subtracting background from the raw perpendicular (S) and parallel (P) measurements, polarization (mP) and anisotropy (r) were calculated with the following equations:

$$mP = ((P - S)/(P + S)) \times 1,000$$
$$r = (P - S)/(P + 2S)$$

Surface-binding analyses via SPR. SPR experiments were performed at 25 °C on a Biacore T100 instrument (GE Healthcare) with a Series S SA chip using a running buffer of 10 mM HEPES pH 7.4, 150 mM NaCl, 3 mM EDTA, 0.05% surfactant P20 with 0.1 mg ml^{-1} BSA. Biotinylated Tir-10_v2 peptide (Biotin-Ahx-EHI-pY-DEVAAD) at 10 ng ml^{-1} was injected at 10 μl min^{-1} over a flow cell for 15 or 90 s to capture ~2 or ~14 response units (RUs), respectively. The reference surface was blank streptavidin alone. Protein analytes were repurified by SEC just before use. A buffer blank paired with each 50 nM analyte (concentration based on molecular weight (MW) of construct, with no regard to the number of SH2 units) was injected at 50 μl min^{-1} with 2 min of association and 3 min of dissociation. On the lower density Tir10_v2 surface (Fig. 3e), buffer was flowed at 50 μl min^{-1} for 1 h after the first tetramer injection, to regenerate the surface. Buffer flow alone was insufficient for regeneration of the higher density surface. Overlay plots of double-referenced data were generated, then normalized for off-rate comparison by dividing each curve by its maximum response in Scrubber2.0b software (BioLogic Software). Maximum binding responses observed on the lower density Tir10_v2 surface were 10, 16 and 22 RUs for free SH2, cTRP-SH2 and cTRP-Spy-SH2, respectively. Responses observed on the higher density Tir10_v2 surface were 80 RUs for free SH2 and 230 RUs for cTRP-Spy-SH2 (data not shown). Figures were made in Prism 7 (GraphPad).

Epitope-specific T-cell staining. Approximately 0.5 × 10^6 clonal CMV pp65-reactive HLA-A*02$^+$CD8$^+$ T cells or healthy PBMCs per sample (authenticated using microscopy morphology checks and short tandem repeat analyses), from an overnight incubation in CTL media (RPMI, 10% heat-inactivated human AB sera, 2% L-glutamine (4 mM), 1% penicillin/streptomycin, 0.01% β-mercaptoethanol (0.5 M))[22], were spun in 5 ml FACS tubes at 1,200 r.p.m. for 10 min at 4 °C, and washed once with wash buffer (Miltenyi autoMACS running buffer). The washed cells were resuspended in 100 μl of wash buffer. cTRP24$_6$SS-scMHC or streptavidin-allophycocyanin (APC)-conjugated scMHC constructs (generated by the Immune Monitoring Core Laboratory at Fred Hutchinson Cancer Research Center) were added at 5 μg ml^{-1} concentration to each sample, mixed well and incubated on ice in the dark for 30 min. Wash buffer (4 ml) was added, the cells were spun down at 1,200 r.p.m. for 10 min at 4 °C and resuspended in 100 μl of wash buffer. A secondary labeling antibody, THE anti-His-iFluor647 (GenScript, catalog no. A01802), was added to 4 μg ml^{-1} samples incubated with the cTRP24$_6$SS-scMHC protein and incubated for a further 30 min. The cells were washed with 4 ml of wash buffer, resuspended in 100 μl of wash or DAPI buffer and

then analyzed on a BD LSR II flow cytometer. Gating strategies were chosen based on their forward and side-scatter properties, single parameter histograms and two-parameter density plots of cell populations.

T-cell isolation, proliferation and activation assays. Human $CD8^+$ T cells were derived from healthy donor PBMCs and isolated following the instructions of the EasySepTM Human Bulk $CD8^+$ T-cell Isolation Kit (Stem Cell, catalog no. 17951). Cells were labeled with CFSE for 10 min at 37 °C and subsequently quenched with FBS before washing. Cells (1×10^5) were resuspended in CTL media supplemented with 50 U ml^{-1} human IL-2 and added to anti-CD3 (OKT3; 5 µg ml^{-1}; BioLegend, catalog no. 317347)-coated (non-TC treated) flat-bottomed 96-well plates in the presence or absence of soluble anti-CD28 (TGN1412; 1 µg ml^{-1}), $cTRP_6SS$-$scTrimer^{CD28}$ (1 µg ml^{-1}) or $cTRP_6SS$-$scTrimer^{CD70}$ (1 µg ml^{-1}). CFSE dilution was assessed 3 d after activation by flow cytometry. Alternatively, CD8 T cells were activated with anti-CD3/anti-CD28 beads (ThermoFisher, catalog no. 11131D) for 4 d. Cells were incubated for 30 min at 37 °C with $cTRP24_6SS$-$scTrimer^{OX40L}$ (2 µg ml^{-1}) or $cTRP24_6SS$-$scTrimer^{4\text{-}1BBL}$ (2 µg ml^{-1}) and subsequently stained at 4 °C using THE anti-His antibody (GenScript, catalog no. A00186). Receptor surface expression was assessed using anti-human OX40 (BioLegend, catalog no. 350007; clone ACT53) and 4-1BB (BioLegend, catalog no. 309803; clone 4B4-1) monoclonal antibodies.

For the NF-κB luciferase reporter assays, Ultra-LEAF purified anti-human CD3 antibody (OKT3) was diluted in 1× DPBS to 50 µl and incubated overnight in a nontissue culture treated round-bottom plate (Corning, catalog no. 3788) at 4 °C. Contents of the plate were drained so as not to disturb the protein monolayer formed in the bottom of each well. Dilution series of the costimulation constructs were prepared in serum-free media (X-Vivo, catalog no. 04-744Q) and added to the plate. Jurkat cells (1×10^5) transduced with an NF-κB luciferase reporter were added to each well and incubated for 24 h at 37 °C. Data were collected using a Biotek Synergy 2 plate reader with autoinjector dispensing coelenterazine (Nanolight Technology, 303-10) dissolved in propylene glycol and diluted to 0.01 mg ml^{-1} in cell media at 25 °C.

Reporting Summary. Further information on research design is available in the Nature Research Reporting Summary linked to this article.

Data availability

The identities and sequences of all constructs used in this study are provided in Supplementary Table 1. All other data described in the article are provided in the main article and Extended Data figures. Source data for Figs. 3d and 5b are available with the paper online.

References

19. Taylor, G. K., Heiter, D. F., Pietrokovski, S. & Stoddard, B. L. Activity, specificity and structure of I-Bth0305I: a representative of a new homing endonuclease family. *Nucleic Acids Res.* **39**, 9705–9719 (2011).
20. Dyer, K. N. et al. High-throughput SAXS for the characterization of biomolecules in solution: a practical approach. *Methods Mol. Biol.***1091**, 245–258 (2014).
21. Scarff, C. A., Fuller, M. J. G., Thompson, R. F. & Iadaza, M. G. Variations on negative stain electron microscopy methods: tools for tackling challenging systems. *J. Vis. Exp.* **132**, e57199 (2018).
22. Warren, E. H., Greenberg, P. D. & Riddell, S. R. Cytotoxic T-lymphocyte-defined human minor histocompatibility antigens with a restricted tissue distribution. *Blood* **91**, 2197–2207 (1998).

Acknowledgements

A. Towlerton and E. H. Warren provided materials, advice and facilitation of scMHC tetramer-based flow cytometric experiments. R. Strong provided advice and facilitation of SPR (Biacore) binding experiments. J. Carter provided operations support for mammalian protein production and J. M. Olson provided laboratory support for protein expression. This work was funded by the NIH (grant no. R01 GM123378) and by the Fred Hutchinson Cancer Research Center.

Author contributions

P.B. conducted the computational protein design work, including fold design and identification of point mutations leading to alteration of self-assembly properties, and generated the structural models used throughout the article. J.H., L.A.D., A.Q., C.P., B.K.K., B.L.S. and R.O.R. all conducted protein expression, purification and biochemical characterization experiments. B.W.S. conducted EM visualization studies. D.J.F. conducted SPR protein-binding studies. Y.X., C.A.J.-R., A.D.B. and S.R.R. designed and conducted T-cell staining studies. C.E.C. and B.L.S. designed functionalized cTRP constructs. C.E.C., B.K.K., B.L.S. and P.B. wrote the manuscript, which was edited extensively by all authors.

Competing interests

C.E.C., P.B., S.R.R. and B.L.S. are employees of the Fred Hutchinson Cancer Research Center; they are named inventors on intellectual property corresponding to the technology in this article. S.R.R. is a founder of Lyell Immunopharma Inc., which has recently licensed the technology for use in T-cell culture applications.

Additional information

Extended data is available for this paper at https://doi.org/10.1038/s41594-020-0397-5.

Supplementary information is available for this paper at https://doi.org/10.1038/s41594-020-0397-5.

Correspondence and requests for materials should be addressed to B.K.K., B.L.S. or P.B.

Peer review information Inês Chen was the primary editor on this article and managed its editorial process and peer review in collaboration with the rest of the editorial team.

Reprints and permissions information is available at www.nature.com/reprints.

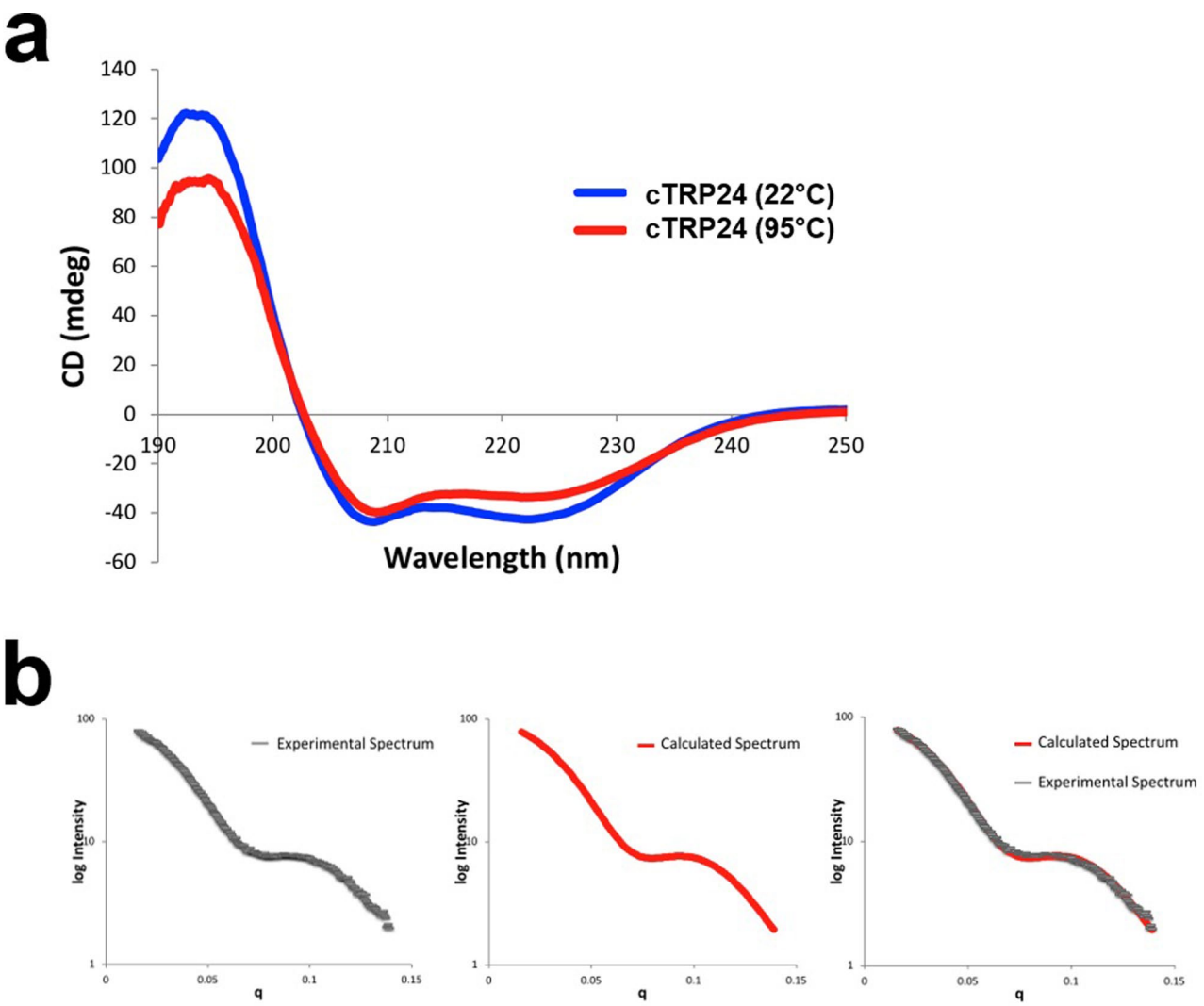

Extended Data Fig. 1 | Characterization of engineered cTRP24. a, Circular dichroism (CD) spectra of cTRP24 at 22° and 95 °C shows preservation of secondary structure at high temperature. **b**, Small angle x-ray scattering (SAXS) spectra measured for cTRP24 (left), calculated SAXS spectrum derived from the atomic model of the designed protein construct (middle) and a superposition of the experimental and calculated spectra (right).

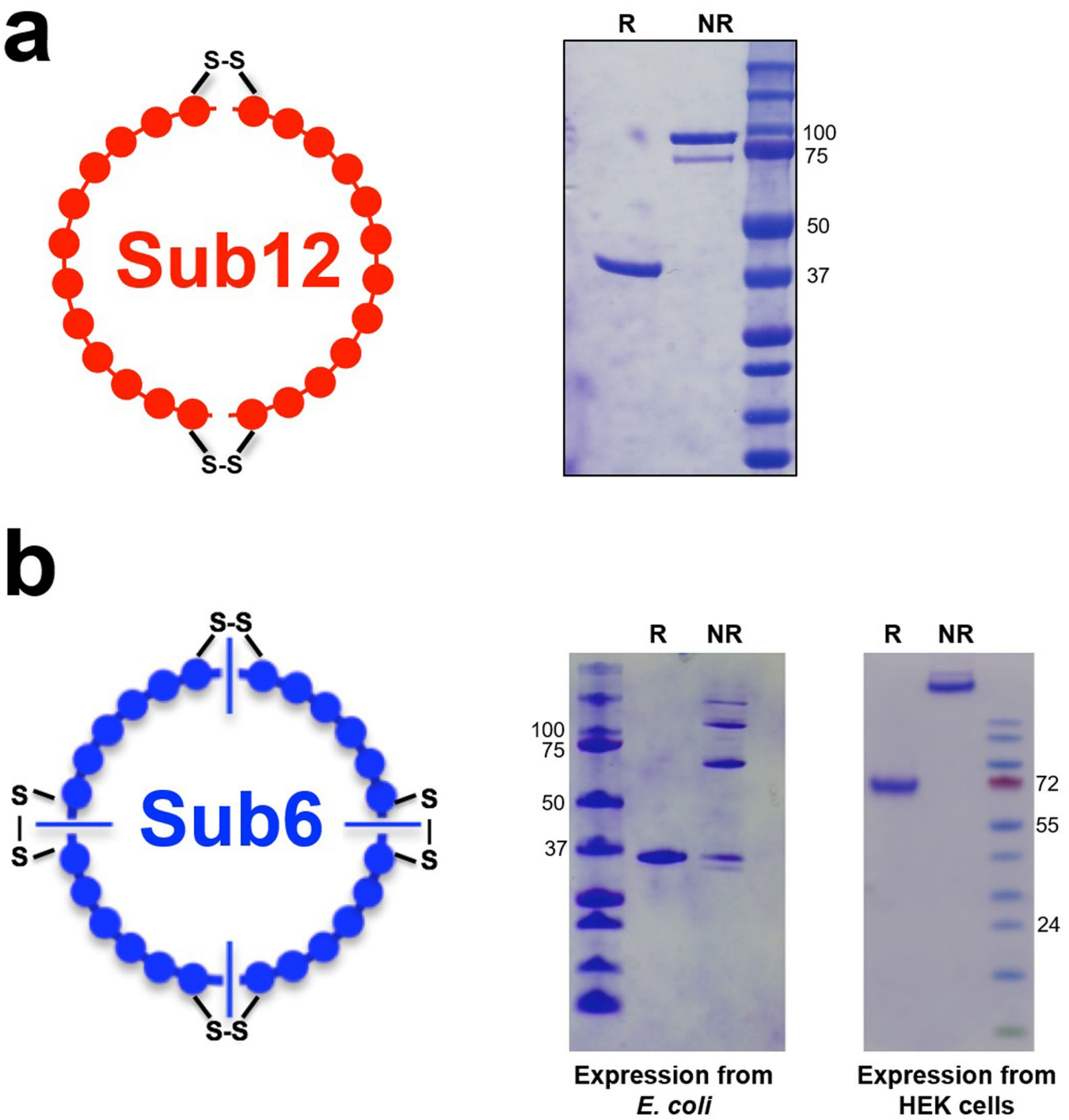

Extended Data Fig. 2 | Design and electrophoretic gel visualization of self-assembling, disulfide-stapled cTRP24 nanoparticles. a, The cTRP2412SS construct, assembled from dimerization of two identical protein subunits each harboring 12 repeats, with the N- and C-terminal repeat of each containing a cysteine residue (described in the main text and in Fig. 2) that enable disulfide stapling. SEC analyses (shown in Fig. 2c) and electrophoretic analyses (right panel) both indicate formation of a dimer that contains a mixture of one or two disulfide staples, both of which behave in solution similarly to a monomeric, single chain 24-repeat cTRP. **b**, A cTRP246SS construct, assembled from four identical protein subunits each harboring 6 repeats, with the N- and C-terminal repeat of each containing a cysteine residue (described in the main text and in Fig. 2) that enable disulfide stapling. SEC analyses indicate that expression and purification yield a cTRP24 that behaves in solution in a similar manner to a monomeric, single chain 24-repeat cTRP. Electrophoretic analyses of the same construct generated either via cytosolic expression in *E. coli* (and then oxidized in the presence of air during purification) or via secretion from human HEK cells (oxidized as part of eukaryotic disulfide bond formation mechanism during secretion) indicate that disulfides are formed in both cases. However, expression from bacteria generates a mixture of species (harboring 2, 3 or 4 disulfides), whereas expression and secretion from human cells generated a more homogeneous population of species primarily consisting of a full complement of disulfide bonds.

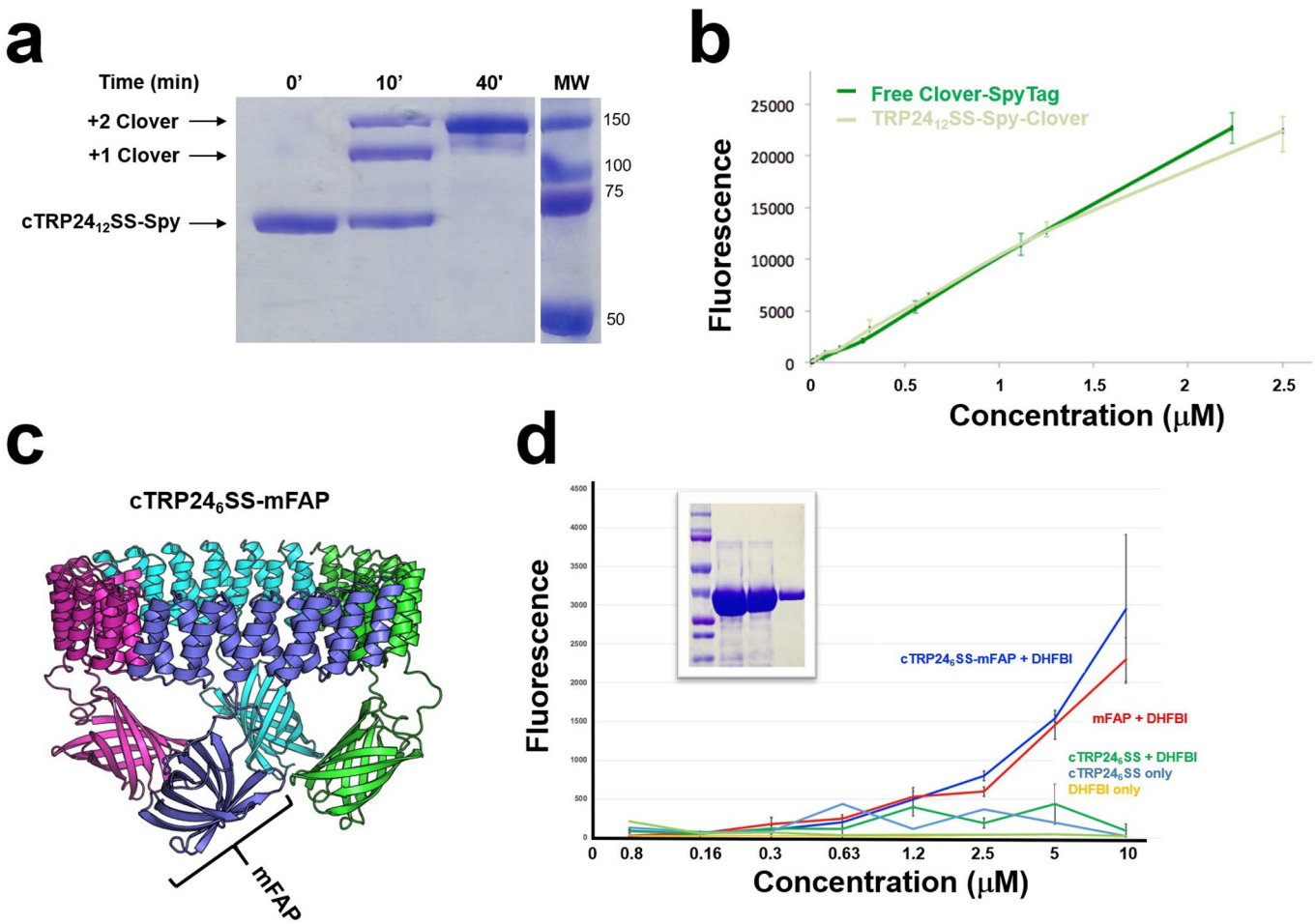

Extended Data Fig. 3 | Functional characterization of additional cTRP constructs. a, A 24-repeat cTRP harboring four copies of the SpyCatcher protein domain (cTRP2412SS-Spy) is fully conjugated with four copies of SpyTagged Clover (a derivative of GFP). In this reducing SDS-PAGE gel two bands are observed as a result of addition of SpyCatcher, corresponding to capture of 1 or 2 copies of SpyTagged Clover by each 12-repeat protein subunit. **b**, Fluorescence of free Clover and cTRP2412SS-Spy-Clover nanoparticles, as a function of normalized Clover concentrations. Data shown as mean and s.d. for n=3 independent experiments. **c**, Four copies an engineered fluorescence activating protein ('mFAP') are inserted into four evenly distributed surface loops around the bottom face of the cTRP ('cTRP246SS-mFAP'). **d**, Purification and fluorescence activity of cTRP246SS-mFAP. mFAP has previously been demonstrated to fluoresce in the presence of exogenous, bound DHFBI fluorophore. The two curves that demonstrate increasing fluorescence as a function of protein concentration correspond to the cTRP246SS-mFAP (blue) nanoparticle and to free mFAP (red); as in panel b the protein concentrations are normalized relative to the one-versus-four copies of mFAP per molecule. The three curves that do not increase in fluorescence as a function of protein concentration correspond to the 'naked' cTRP (cTRP246SS), cTRP246SS plus DHFBI, and DHFBI alone. For the latter two constructs, the DHFBI concentration is equivalent at each protein concentration to that which is present in the active constructs. Data shown as mean and s.d. for n=3 independent experiments.

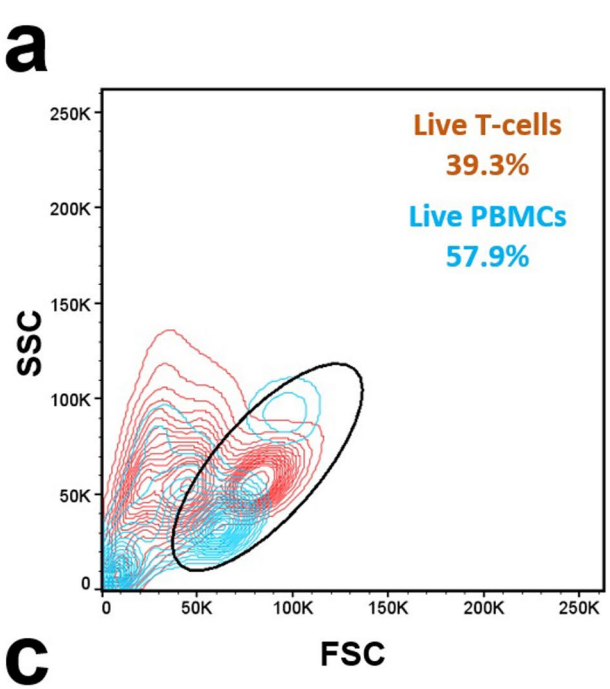

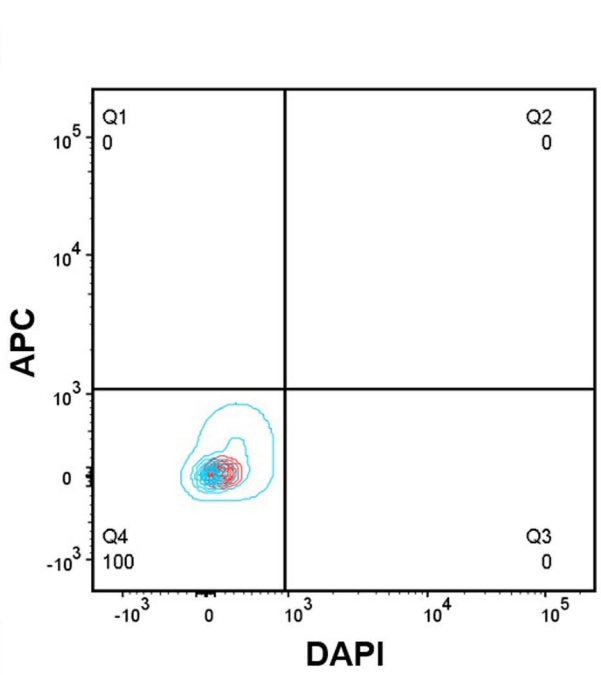

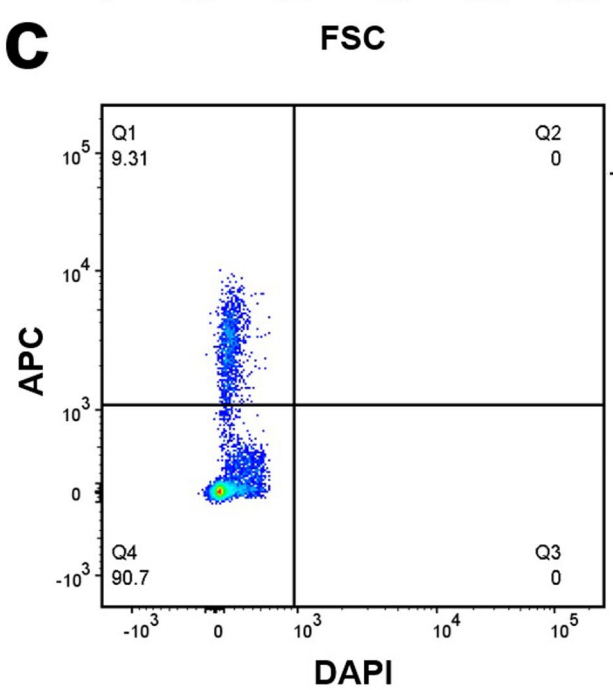

d

CMV:PBMC	cTRP24$_6$SS-scMHC	SA-Tetramer
CMV Only	87.1%	98.7%
1:4	9.3%	10.1%
1:20	1.6%	2.0%
1:100	0.6%	0.5%

Extended Data Fig. 4 | Detection of CMV pp65-reactive CD8$_+$ T-cells diluted into donor PBMCs using cTRP24$_6$SS-scMHC and streptavidin-allophycocyanin (APC) tetramers. a, Forward versus side scatter plot showing an overlay of CMV pp65-reactive T-cells (red contour plot) and donor PBMCs (blue contour plot) and the lymphocyte gating strategy used for further analysis. This strategy was used to quantitate CMV pp65-reactive T-cells diluted into donor PBMCs as shown in panels **c** and **d**. **b**, Scatter plot showing an overlay of the DAPI-negative lymphocyte gates stained with an anti-His-APC secondary antibody (Biolegend #362605) confirms that the secondary antibody used to detect cTRP246SS-scMHC does not result in unwanted background staining of live cells. **c**, Representative flow cytometry scatter plot showing quantitation of CMV pp65-reactive T-cells diluted into donor PBMCs at a ratio of 1:4 respectively. **d**, Quantitation of CMV pp65-reactive T-cells at various dilutions using both the cTRP246SS-scMHC (detected using the anti-His-APC secondary) and streptavidin-APC scMHC tetramer (SA-Tetramer). Note that the ratios in the first column (CMV:PBMC) represent raw cell counts prior to staining.

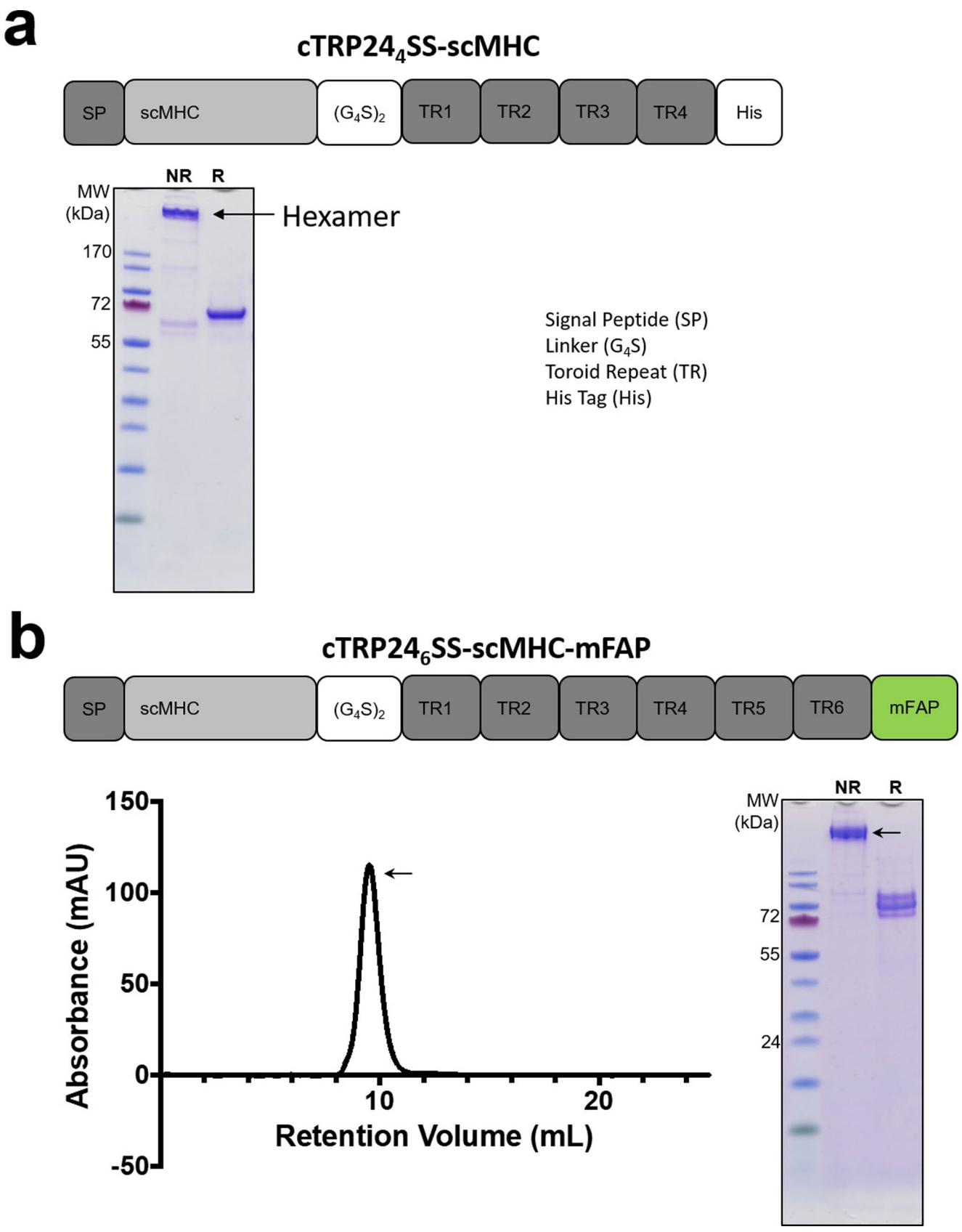

Extended Data Fig. 5 | Expression and preliminary characterization of a hexameric cTRP24 harboring N-terminal cargo and a tetrameric cTRP24 harboring both N- and C-terminal cargos. a, Schematic showing the architecture of the cTRP244SS-scMHC and corresponding non-reducing and reducing SDS-PAGE following affinity purification. Under reducing conditions, the protein migrates as a monomer. **b**, Schematic showing the architecture of the cTRP246SS-scMHC-mFAP protein displaying four copies of a scMHC at each N-terminus and four copies of mFAP at each C-terminus, both decorating top of the cTRP scaffold. SEC and corresponding SDS-PAGE analysis confirms proper assembly of a functional tetramer.

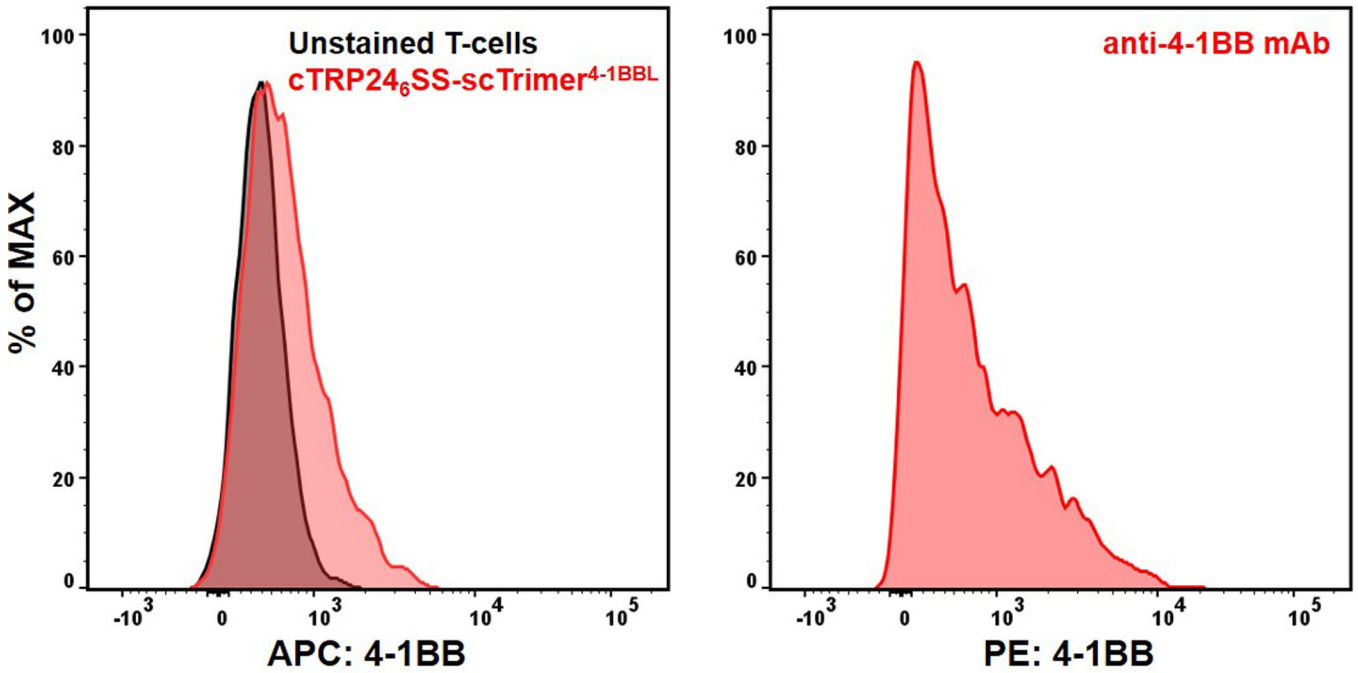

Extended Data Fig. 6 | Staining of 4-1BB receptor on activated CD8$_+$ T-cells using cTRP24$_6$SS-scTrimer$_{4\text{-}1BBL}$. Flow cytometry histogram showing staining of activated CD8+ T-cells (4 days post stimulation with anti-CD3/anti-CD28 beads) with cTRP246SS-scTrimer4-1BBL using a secondary anti-His-iFluor647 antibody or unstained T cells (left) and a PE-labeled anti-4-1BB mAb (right).

nature research

Corresponding author(s): Brett Kaiser, Barry Stoddard and Phil Bradley

Last updated by author(s): Dec 18, 2019

Reporting Summary

Nature Research wishes to improve the reproducibility of the work that we publish. This form provides structure for consistency and transparency in reporting. For further information on Nature Research policies, see Authors & Referees and the Editorial Policy Checklist.

Statistics

For all statistical analyses, confirm that the following items are present in the figure legend, table legend, main text, or Methods section.

n/a	Confirmed	
☒	☐	The exact sample size (*n*) for each experimental group/condition, given as a discrete number and unit of measurement
☒	☐	A statement on whether measurements were taken from distinct samples or whether the same sample was measured repeatedly
☒	☐	The statistical test(s) used AND whether they are one- or two-sided *Only common tests should be described solely by name; describe more complex techniques in the Methods section.*
☒	☐	A description of all covariates tested
☒	☐	A description of any assumptions or corrections, such as tests of normality and adjustment for multiple comparisons
☒	☐	A full description of the statistical parameters including central tendency (e.g. means) or other basic estimates (e.g. regression coefficient) AND variation (e.g. standard deviation) or associated estimates of uncertainty (e.g. confidence intervals)
☒	☐	For null hypothesis testing, the test statistic (e.g. *F*, *t*, *r*) with confidence intervals, effect sizes, degrees of freedom and *P* value noted *Give P values as exact values whenever suitable.*
☒	☐	For Bayesian analysis, information on the choice of priors and Markov chain Monte Carlo settings
☒	☐	For hierarchical and complex designs, identification of the appropriate level for tests and full reporting of outcomes
☒	☐	Estimates of effect sizes (e.g. Cohen's *d*, Pearson's *r*), indicating how they were calculated

Our web collection on statistics for biologists contains articles on many of the points above.

Software and code

Policy information about availability of computer code

Data collection	*Provide a description of all commercial, open source and custom code used to collect the data in this study, specifying the version used OR state that no software was used.*
Data analysis	Scrubber2.0b software (BioLogic Software) for Surface Plasmon Resonance analyses; FlowJo 10.6.1 software for all flow cytometry data processing; PyMOL for creation of molecular models; GraphPad Prism 8 for all other data analysis

For manuscripts utilizing custom algorithms or software that are central to the research but not yet described in published literature, software must be made available to editors/reviewers. We strongly encourage code deposition in a community repository (e.g. GitHub). See the Nature Research guidelines for submitting code & software for further information.

Data

Policy information about availability of data

All manuscripts must include a data availability statement. This statement should provide the following information, where applicable:

- Accession codes, unique identifiers, or web links for publicly available datasets
- A list of figures that have associated raw data
- A description of any restrictions on data availability

The amino acid sequences of all constructs used in the study are provided in the text (Supplementary Table 1). No additional data sets beyond those in the figures require deposition.

Field-specific reporting

Please select the one below that is the best fit for your research. If you are not sure, read the appropriate sections before making your selection.

☒ Life sciences ☐ Behavioural & social sciences ☐ Ecological, evolutionary & environmental sciences

For a reference copy of the document with all sections, see nature.com/documents/nr-reporting-summary-flat.pdf

Life sciences study design

All studies must disclose on these points even when the disclosure is negative.

Sample size	*Describe how sample size was determined, detailing any statistical methods used to predetermine sample size OR if no sample-size calculation was performed, describe how sample sizes were chosen and provide a rationale for why these sample sizes are sufficient.*
Data exclusions	*Describe any data exclusions. If no data were excluded from the analyses, state so OR if data were excluded, describe the exclusions and the rationale behind them, indicating whether exclusion criteria were pre-established.*
Replication	All binding, cell staining experiments and T cell activation/proliferation assays (Figures 4, 5 and 6) were conducted in triplicate using independent aliquots of proteins, cells and ligands. Error bars represent standard deviation.
Randomization	*Describe how samples/organisms/participants were allocated into experimental groups. If allocation was not random, describe how covariates were controlled OR if this is not relevant to your study, explain why.*
Blinding	*Describe whether the investigators were blinded to group allocation during data collection and/or analysis. If blinding was not possible, describe why OR explain why blinding was not relevant to your study.*

Reporting for specific materials, systems and methods

We require information from authors about some types of materials, experimental systems and methods used in many studies. Here, indicate whether each material, system or method listed is relevant to your study. If you are not sure if a list item applies to your research, read the appropriate section before selecting a response.

Materials & experimental systems

n/a	Involved in the study
☐	☒ Antibodies
☐	☒ Eukaryotic cell lines
☒	☐ Palaeontology
☒	☐ Animals and other organisms
☒	☐ Human research participants
☒	☐ Clinical data

Methods

n/a	Involved in the study
☒	☐ ChIP-seq
☐	☒ Flow cytometry
☒	☐ MRI-based neuroimaging

Antibodies

Antibodies used	anti-human CD3 (BioLegend #317347; Clone OKT3); anti-human CD28 (Internal Reagent; Clone TGN1412); anti-human OX40 (BioLegend #350007; Clone ACT53) and anti-human 4-1BB (BioLegend #309803; Clone 4B4-1); anti-His (Genscript #A01802; Clone THE His)
Validation	All primary and secondary antibodies used in the studies were validated in control experiments prior to use and titrated based on manufacturer recommendations.

Eukaryotic cell lines

Policy information about cell lines

Cell line source(s)	Freestyle 293-F Cells (ThermoFisher# R79007); clonal CMV pp65-reactive HLA-A*02+CD8+ T-cells from the Edus Warren lab (Fred Hutch Clinical Research Division), PBMC-derived T cells purified from multiple donors (Fred Hutch Clinical Research Division)
Authentication	Morphology check by microscope; STR analysis
Mycoplasma contamination	All cell lines tested negative for mycoplasma contamination.

Commonly misidentified lines (See ICLAC register)	*Name any commonly misidentified cell lines used in the study and provide a rationale for their use.*

Flow Cytometry

Plots

Confirm that:

☒ The axis labels state the marker and fluorochrome used (e.g. CD4-FITC).

☒ The axis scales are clearly visible. Include numbers along axes only for bottom left plot of group (a 'group' is an analysis of identical markers).

☐ All plots are contour plots with outliers or pseudocolor plots.

☐ A numerical value for number of cells or percentage (with statistics) is provided.

Methodology

Sample preparation	Clonal CMV pp65-reactive HLA-A*02+CD8+ T-cells were spun in 5 mL FACS tubes at 1200 RPM for 10 minutes at 4°C, and washed 1 time with wash buffer (Miltenyi autoMACS running buffer, Miltenyi). The washed cells were resuspended in 100 uL of wash buffer. Naive CD8+ T cells were purified from donor PBMCs using manufacturer protocols (StemCell# 17951)
Instrument	BD LSR II flow cytometer (BD biosciences).
Software	FlowJo 10.6.1
Cell population abundance	500,000 clonal CMV pp65-reactive HLA-A*02+CD8+ T-cells per sample; purity assessed via microscopy and flow cytometry (FSC/SSC).
Gating strategy	For all flow cytometry data, initial FSC/SSC gates were drawn to include healthy lymphocyte populations and exclude dead/dying cells or cell debris. In Figure 4d and Supplementary Figure 4, a secondary gate was applied to exclude DAPI+ cells and tetramer staining is shown as a single parameter histogram. Where anti-His-Fluor secondary antibodies were used for detection, gating strategies are shown with the secondary antibody alone to confirm low background staining. CFSE-based proliferation data is shown as single parameter histograms for clarity and all other data is shown as two-parameter density plots.

☒ Tick this box to confirm that a figure exemplifying the gating strategy is provided in the Supplementary Information.